J. Fluid Mech. (1979), *vol.* 90, *part* 1, *pp.* 67–107
Printed in Great Britain

The influence of suction on the structure of turbulence in fully developed pipe flow

By M. SCHILDKNECHT, J. A. MILLER† AND G. E. A. MEIER

Max-Planck-Institut für Strömungsforschung,
Göttingen, West Germany

(Received 30 April 1977 and in revised form 29 June 1978)

The effect of uniform wall suction on the structure of turbulence in a fully established turbulent pipe flow has been measured, with special attention to the critical layers close to the wall. Uniform suction was introduced into a pipe flow with a Reynolds number of 17250 by means of a porous-walled section 2·2 diameters in length with very fine perforations. The effect of suction on the turbulent energy balance was then measured over the entire cross-section at four axial locations. The results indicate the following.

(i) The amplitudes of the three principal velocity fluctuation components are reduced by suction, but to differing degrees. Moreover, the effects of suction on the amplitudes of these fluctuations develop at differing rates such that the x-wise components are first affected, then the r-wise and lastly the ϕ-wise components.

(ii) The suction-induced perturbation in the turbulent structure propagates from the wall to the pipe centre-line with a velocity approximately equal to the friction velocity U_τ.

(iii) Even with very small rates of fluid extraction the maxima of the terms in the turbulent energy balance occurring close to the wall are drastically reduced. Nevertheless there is no tendency for the location of these maxima to move towards the wall.

(iv) The general reduction of the level of turbulent energy across the entire section is due to transport of this energy by the augmented mean radial velocity towards the wall, where it is dissipated since the boundary condition inhibits the passage of turbulent energy through the wall.

1. Introduction

Insight into the mechanism of boundary-layer suction is of special interest in technical applications because, as is well known, suction influences transition, separation and heat-transfer rates. Unfortunately the numerous theoretical and experimental investigations reported in the literature are concerned principally with the influence of wall suction on laminar flows or on the macroscopic properties of turbulent flows. Weissberg & Bergman (1955) studied the influence of suction on turbulent velocity fluctuations. Applying uniform suction to a fully established turbulent pipe flow for a range of exit Reynolds numbers from 27×10^3 to 79×10^3, they found that the effect of suction was to reduce the streamwise velocity fluctuation, normalized with the

† Present address: Naval Postgraduate School, Monterey, California.

local mean velocity, at all radial locations. In the experiments of Aggarwal, Hollingsworth & Mayhew (1972) uniform wall suction was applied to a fully established turbulent pipe flow for a length of 10 pipe diameters. It was found in this investigation that turbulent intensities, normalized with the local mean velocity, decreased in the central core at very low suction rates but increased at higher suction rates; however the absolute level of turbulent fluctuation was always found to be reduced by suction. More recently Brosch & Winograd (1974) have reported similar results of the effects of suction on turbulent pipe flows. Aurelli (1967) was able to infer the Reynolds stresses from measurements of mean flow properties in a fully established turbulent pipe flow with wall suction and found that the Reynolds stress was decreased by the application of suction.

Favre (1966) reported some fluctuation measurements for flow in a turbulent boundary layer over a flat plate with uniform suction. Direct measurement of turbulent fluctuations and the Reynolds shear stress demonstrated decreasing values of these quantities with increasing suction rates and increasing distances from the leading edge of the porous wall.

Theoretical models for calculating mean velocity profiles in turbulent pipe flow with wall suction have been proposed by Kinney & Sparrow (1970) and Merkine, Solan & Winograd (1971). Rotta (1966) has addressed the question of the influence of suction on the turbulent energy balance in a theoretical investigation of the flow over a porous flat plate in which he attempted to estimate the magnitude of the various terms in the turbulent energy equation.

In the present work an attempt has been made to determine the influence of wall suction on the structure of turbulence in a fully established pipe flow through direct hot-wire measurement of the fluctuating energy terms appearing in the turbulent energy equation.

2. The turbulent energy equation

From the continuity and momentum equations for incompressible flow one may obtain the normalized energy equation for turbulent fluctuations in cylindrical co-ordinates:

$$\begin{aligned}
&\frac{D}{U_\tau^3}\left\{\overline{u^2}\frac{\partial U}{\partial x}+\overline{uv}\left(\frac{\partial U}{\partial x}+\frac{\partial U}{\partial r}\right)+\overline{v^2}\frac{\partial V}{\partial r}+\overline{Vw^2}\right\}\\
&\quad+\frac{D}{U_\tau^3}\left\{\frac{\partial}{\partial x}U\left(\overline{\frac{u^2+v^2+w^2}{2}}\right)+\frac{1}{r}\frac{\partial}{\partial r}rV\left(\overline{\frac{u^2+v^2+w^2}{2}}\right)\right\}\\
&\quad+\frac{D}{U_\tau^3}\left\{\frac{\partial}{\partial x}u\left(\overline{\frac{u^2+v^2+w^2}{2}+\frac{p}{\rho}}\right)+\frac{1}{r}\frac{\partial}{\partial r}rv\left(\overline{\frac{u^2+v^2+w^2}{2}+\frac{p}{\rho}}\right)\right\}\\
&\quad-\frac{\nu D}{U_\tau^3}\left\{\frac{\partial^2}{\partial x^2}\left(\overline{\frac{u^2+v^2+w^2}{2}}\right)+\frac{1}{r}\frac{\partial}{\partial r}r\frac{\partial}{\partial r}\left(\overline{\frac{u^2+v^2+w^2}{2}}\right)\right\}\\
&\quad+\frac{D}{U_\tau^3}\left\{\overline{\left(\frac{\partial u}{\partial x}\right)^2}+\overline{\left(\frac{\partial u}{\partial r}\right)^2}+\frac{1}{r^2}\overline{\left(\frac{\partial u}{\partial \phi}\right)^2}+\overline{\left(\frac{\partial v}{\partial x}\right)^2}+\frac{1}{r^2}\overline{\left(\frac{\partial v}{\partial \phi}\right)^2}+\overline{\left(\frac{\partial w}{\partial x}\right)^2}\right.\\
&\qquad\left.+\overline{\left(\frac{\partial w}{\partial r}\right)^2}+\frac{1}{r^2}\overline{\left(\frac{\partial w}{\partial \phi}\right)^2}-\frac{4}{r^2}\overline{w\frac{\partial v}{\partial \phi}+\frac{v^2+w^2}{r^2}}\right\}=0,
\end{aligned}$$

in which we have taken as the origin of the cylindrical co-ordinate system (x, r, ϕ) the axis at the entrance plane of the porous-walled tube. The mean velocity components corresponding to x, r and ϕ are U, V and W, and the fluctuating velocity components are u, v and w. The normalizing parameters are the kinematic viscosity ν, the friction velocity U_τ for a smooth pipe and the pipe diameter D.

The boundary conditions are

$$U = W = 0, \quad V \neq 0, \quad u = v = w = 0$$

at the wall $r = \frac{1}{2}D$ and

$$\partial v/\partial r = 0, \quad \overline{uv} = 0$$

at the centre-line $r = 0$.

The terms included in the energy equation may be identified with certain physical phenomena. Accordingly, the first term may be called the turbulent energy production, the second the turbulent energy convection attributable to the mean motion, the third the turbulent energy convection attributable to the fluctuating motion, the fourth the turbulent energy diffusion and the last the turbulent energy dissipation. Some writers (Laufer 1953) have referred to the third term, excluding the velocity–pressure correlations, as the turbulent kinetic energy diffusion rate, the velocity–pressure correlations being referred to as the turbulent pressure–energy diffusion rate, and to the fourth term as the gradient diffusion rate of turbulent kinetic energy.

In the present study, where the wall suction is uniform and independent of the co-ordinate ϕ, the derivatives of quantities averaged with respect to ϕ must vanish and accordingly do not appear in the energy equation.

Because the Reynolds number formed from the wall friction velocity and the perforation diameter is less than unity we may infer that the wall is impermeable to turbulent energy and that the behaviour of the velocity fluctuations in the neighbourhood of the wall must be similar to that near a solid wall. One may use this to develop some information concerning the behaviour of the turbulent energy in the wall layers. If the components of the velocity fluctuation are expanded in a power series in terms of the wall distance r', it follows from the boundary condition discussed above that the series must vanish at the wall. Thus the constant term in the series must vanish identically. From the measurements of Eckelmann (1974) it is known that fluctuations in the molecular shear stress exist in the wall layers for the velocity components parallel to the wall and it follows that the series representing these velocity components must begin with a linear term. Using the continuity equation, one may demonstrate that for the normal velocity component a series representation must begin with a quadratic term. Thus for the fluctuating components near the wall we may write

$$u = a_1(x, \phi, t)\, r' + \ldots,$$
$$v = b_2(x, \phi, t)\, r'^2 + \ldots,$$
$$w = c_1(x, \phi, t)\, r' + \ldots.$$

If one now substitutes these series representations into the energy equation it is found that the first three terms, representing turbulent energy production, convection and diffusion, must vanish at the wall; however the fourth term, the gradient diffusion rate of turbulent energy, as well as the quantities $\overline{(\partial u/\partial r)^2}$ and $\overline{(\partial w/\partial r)^2}$ appearing in the fifth term, the dissipation, need not vanish at the wall. It follows then that

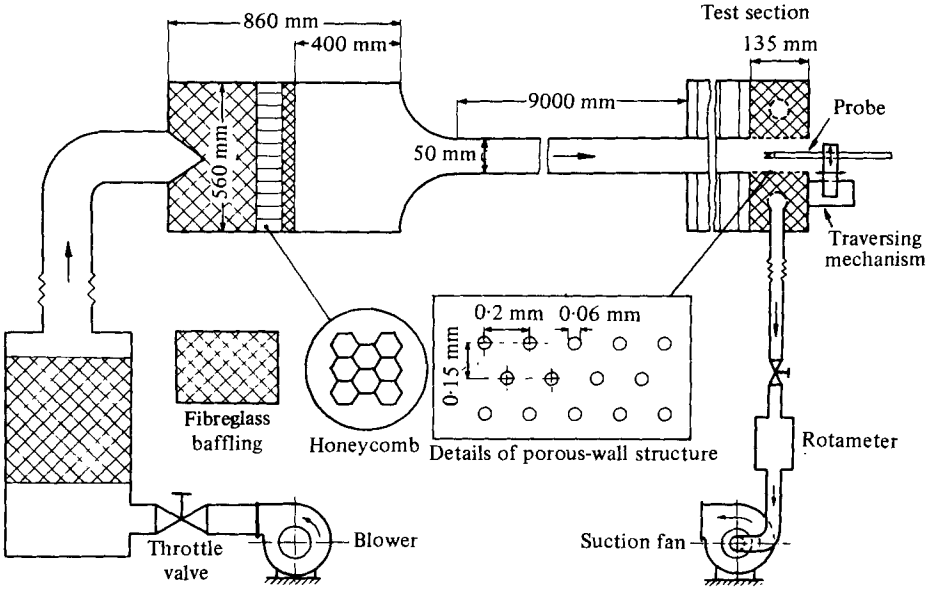

FIGURE 1. Experimental apparatus.

measurements of these quantities must be carried out in the wall layers as close as is practicable to the solid boundary itself.

3. Experimental facilities

All the measurements were carried out in air in the apparatus shown in figure 1. The flow channel consists of a precision glass tube 5·0 cm in diameter and 9 m long fed from a plenum chamber through a nozzle with a contraction ratio of 120. Air was supplied from a radial fan driven by a variable-speed motor. In order to facilitate the hot-wire measurements the air was passed through filters to remove airborne particles before being damped by means of screens and honeycombs in the plenum chamber. A circumferential boundary-layer trip consisting of a 2 cm strip of sandpaper at the tube inlet ensured a fully developed turbulent velocity profile well upstream of the test section.

Suction was introduced into the test section over a length of 13·5 cm by means of a porous nickel tube 5 cm in diameter. The nickel tube was fabricated electrolytically with holes 0·06 mm in diameter arranged in the pattern detailed in figure 1. The dimensionless hole diameter dU_τ/ν of 1·2 leads to a behaviour without suction similar to that of a smooth wall, according to the measurements of Colebrook & White (1937). Uniform wall suction around the periphery was ensured by the use of a large circumferential plenum surrounding the porous section which contained very dense baffling. Air was withdrawn through a toroidal perforated pipe within the baffled plenum by a suction blower driven by a controllable d.c. motor. The suction mass flow rate was measured with calibrated rotameters.

Hot-wire and Pitot probes were mounted downstream of the test section and were positioned by traversing mechanisms of the type employed on optical benches. Provision was made to allow two separate probes to be moved independently in the

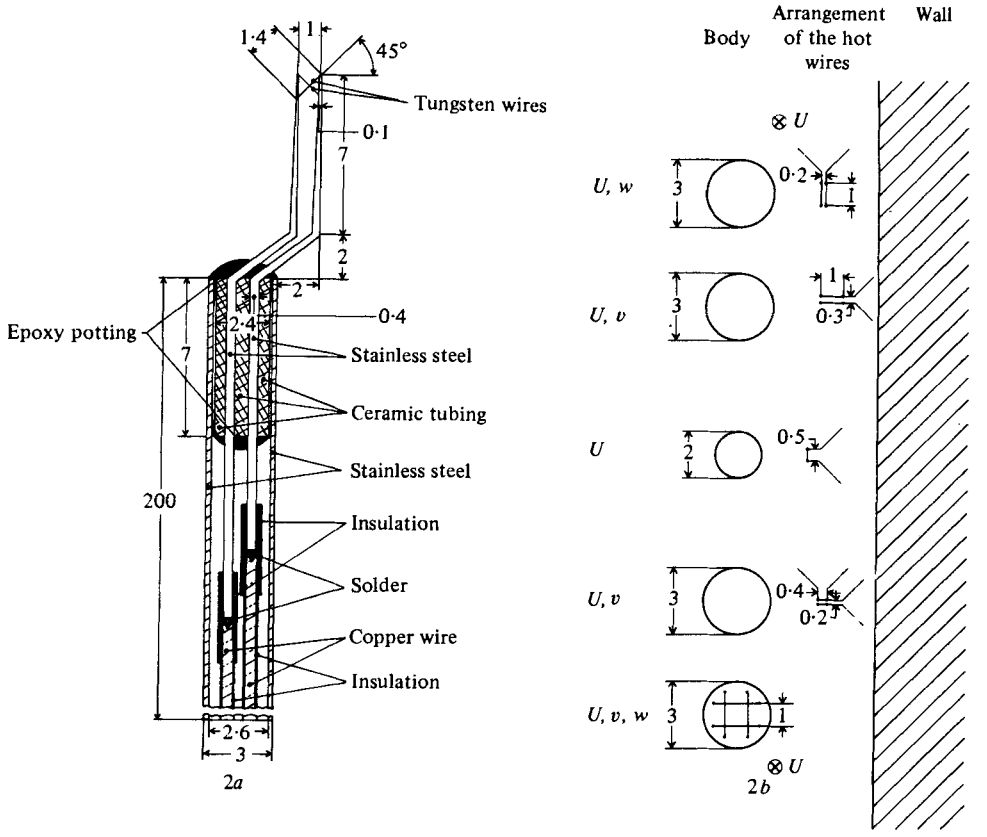

FIGURE 2. Hot-wire probe construction details. Dimensions in mm.

axial, radial and circumferential directions, enabling x, r and ϕ gradients of the fluctuation components and their moments to be measured directly. The estimated accuracy of the position of the traversing mechanism is 0·01 mm in linear displacement and 1′ of arc in rotational displacement.

In order to carry out measurements very close to the wall special probes, not commercially available, were designed and fabricated by the technicians of the Max Planck Institute. A typical probe is detailed in figure 2(*a*) and the hot-wire geometries of each of the probes employed is shown in figure 2(*b*). In order to minimize probe-induced flow perturbations all the probes (with the exception of a four-wire probe used to measure $\overline{w^2v}$) had the wire supports offset with respect to the probe body as shown in figure 2. All the probes were equipped with tungsten wires of either 5·0 or 2·5 μm diameter. These were copper plated at the ends and soft soldered to the supports.

The larger probes detailed in figure 2(*b*) were used in the initial investigation of the effect of the suction rate. The smaller probes were developed in order to measure directly spatial derivatives of the turbulent moments such as $\overline{(\partial u/\partial r)^2}$ and $\overline{(\partial u/\partial \sigma)^2}$ and to approach the wall as closely as possible. The results for the turbulent energy distribution at a fixed suction rate are derived from measurements made with the smaller probes. The four-wire probe, which was employed only for the necessary triple correlation, lacked an offset in the body and was restricted to measurements at

$y^+ > 32$. In this range measurements of $\overline{uv}$ differed from measurements of this quantity made with a conventional X-wire probe by less than 7 %, which provides an estimate of the effects of probe blockage.

Also of concern is the effect of flow angularity on hot-wire probes in the wall layers. For the bulk of the data reported here a 4 % suction rate was adopted, which produced a mean radial velocity at the wall of $V/U_\tau = 0{\cdot}083$, about the same as the local value actually measured at $x/D = 0{\cdot}503$. At $y^+ = 2$ a flow angle of 2·5° with respect to the centre-line results. At $x/D \geqslant 1{\cdot}3$ the corresponding flow angle is about 1·25° because of the reduced local radial velocities. At the greatest suction rate investigated (13 %) these angles might reasonably be expected to be about three times the above values.

Four channels of Disa type 55 M D1 hot-wire bridges and type 55 D10 linearizers were employed in the measurements. The output signals were processed by standard analog techniques to obtain the required correlation functions using laboratory-fabricated electronic circuitry.

A standard square-wave response test, carried out with no flow, indicated that the upper bound of system frequency response for hot wires of diameter 5·0 μm was 29 kHz. The 2·5 μm wires would of course produce an even higher response. The frequency range of the analog differentiator was measured using a sinusoidal signal source and found to be linear from 3 Hz to 3 kHz. A high-pass filter was used to provide a sharp cut-off at 0·5 Hz in the signal processor. Integrating digital voltmeters were used to time average signals. A gate period of 1 min, corresponding to 30 periods of the lowest frequency analysed, was adopted for all measurements of fluctuating quantities.

Although there is no assumption of isotropy, it may be instructive to examine the Kolmogorov length and frequency:

$$l_k \equiv \left(\frac{\nu^3}{\epsilon}\right)^{\frac{1}{4}} = \frac{yu^{\frac{1}{4}}}{y^{+\frac{3}{4}}}, \quad f_k \equiv \left(\frac{\epsilon}{\nu}\right)^{\frac{1}{2}} = \frac{\nu g^{+\frac{3}{2}}}{u^{\frac{1}{2}}y^2}$$

for pipe flow, assuming $\epsilon \cong U_\tau^3/ug$. At the centre-line of the test section, these quantities take on the values

$$l_k = 0{\cdot}9\,\text{mm}, \quad f_k = 500\,\text{Hz}.$$

From the first of these we may calculate the ratio of the hot-wire length l_H to the Kolmogorov length l_k:

$$l_H/l_k = \begin{cases} 5{\cdot}32 & \text{for } 5\,\mu\text{m wires}, \\ 2{\cdot}66 & \text{for } 2{\cdot}5\,\mu\text{m wires}. \end{cases}$$

Overall system calibration was carried out *in situ* using a 1 kHz square wave as a surrogate hot-wire signal. Calibration of the probes was carried out in the test section. The smallest feasible wall distance was determined for each probe by means of a stereo microscope fitted with a measuring reticle at a reference axial position located half a diameter from the exit station $x/D = 2{\cdot}2$. At this position the hot-wire output for a flow without suction was noted and positioning of the probe at axial stations outside the range of the microscope was carried out by matching the respective hot-wire outputs to this reference value.

The existence of truly axisymmetric flow was confirmed by both diametral

traverses at $x/D = 2{\cdot}2$ with and without wall suction, and circumferential traverses at fixed radii. Because of the construction of the porous wall section (detailed above), in which the holes in the toroidal pipe are small compared with the cross-sectional area of the pipe, the pressure drop in the pipe is small compared with that across the holes, which tends to ensure the uniform circumferential suction indicated by the traverses.

The Reynolds number and friction velocity U_τ were inferred from measurements of the pressure drop and total pressure in the unperforated approach section and therefore correspond to conditions of fully developed turbulent flow at the entrance to the test section. The value of U_τ so determined was 0·29 m/s at a Reynolds number of 17 250 based on the measured mass flow at the inlet to the test section.

4. Measurement techniques and data reduction

The first four terms of the energy equation, with the exception of the quantities

$$\overline{\frac{\partial}{\partial x}\left(\frac{up}{\rho}\right)}, \quad \frac{1}{r}\overline{\frac{\partial}{\partial r}\left(\frac{vp}{\rho}\right)},$$

may be obtained directly from measurements of the mean velocity components and the moments $\overline{u^2}$, $\overline{v^2}$, $\overline{w^2}$, $\overline{uv}$, $\overline{u^3}$, $\overline{uv^2}$, $\overline{uw^2}$, $\overline{u^2v}$, $\overline{v^3}$, $\overline{vw^2}$ and their spatial derivatives with respect to x and r. All of these moments were measured directly with the instrumentation described previously. The spatial derivatives were obtained graphically from plots of the respective moments. The pressure correlations were not measured and constitute a portion of the remainder term in the energy balance.

Turning to the dissipation term, one finds considerable difficulty in a direct determination of all of its components. The quantity

$$\overline{\frac{(v^2+w^2)}{r^2}} - \frac{4}{r^2}\overline{\left(w\frac{\partial v}{\partial \phi}\right)},$$

however, can be shown from the hot-wire measurements to be two orders of magnitude smaller than the remaining components of the dissipation term and may be neglected without serious error.†

The streamwise derivatives $\overline{(\partial u/\partial x)^2}$, $\overline{(\partial v/\partial x)^2}$ and $\overline{(\partial w/\partial x)^2}$ appearing in the dissipation term were evaluated by differentiating the signals $u(x, r, \phi, t)$, $v(x, r, \phi, t)$ and $w(x, r, \phi, t)$ with respect to time and employing the method of Townsend (1947):

$$\overline{\left(\frac{\partial u}{\partial x}\right)^2} \cong \overline{\left(\frac{1}{U}\frac{\partial u}{\partial t}\right)^2}.$$

† The second term in this expression may be written, using continuity, as

$$\frac{1}{r}\overline{w\frac{\partial v}{\partial \phi}} = \overline{v\frac{\partial u}{\partial x}} + \frac{\overline{v^2}}{r} + \frac{\partial}{\partial r}\frac{\overline{v^2}}{2} + \frac{1}{r}\frac{\partial\overline{(vw)}}{\partial \phi}.$$

Use of Townsend's hypothesis then gives

$$\overline{v\frac{\partial u}{\partial x}} = \overline{\frac{v}{U}\frac{\partial u}{\partial t}},$$

which permits direct assessment of all terms.

These quantities are significantly smaller than the dominant quantities in the dissipation term and the approximation does not seriously affect the accuracy of the result.

The terms $\overline{(\partial u/\partial r)^2}$ and $\overline{(\partial u/\partial \phi)^2}$ are obtained from the measurements using the relations

$$\overline{\left(\frac{\partial u}{\partial r}\right)^2} \equiv \lim_{\Delta r \to 0} \frac{\overline{u^2(r) + u^2(r+\Delta r) - 2u(r)\,u(r+\Delta r)}}{\Delta r^2},$$

$$\overline{\left(\frac{\partial u}{\partial \phi}\right)^2} \equiv \lim_{\Delta \phi \to 0} \frac{\overline{u^2(\phi) + u^2(\phi+\Delta\phi) - 2u(\phi)\,u(\phi+\Delta\phi)}}{\Delta \phi^2}.$$

Employing two miniature hot-wire probes and the differential traversing mechanisms described above, the correlations appearing in these expressions were measured for a sequence of Δr's and $\Delta\phi$'s and extrapolated to zero. The minimum separation distances are dictated by probe geometry and for the probes employed here were typically $\Delta r = 0{\cdot}2$ mm and $\Delta\phi = 1^\circ\ 30'$. Because of wall thermal interaction and flow distortion, measurements were limited to values of the dimensionless wall distance $r'^+ \geqslant 2{\cdot}0$.

The r- and ϕ-wise spatial derivatives of v and w appearing in the dissipation term could not be measured directly since the cross-wire probe geometries necessary precluded separation distances small compared with the probe dimensions. Thus the terms

$$\overline{\left(\frac{\partial v}{\partial r}\right)^2}, \quad \overline{\left(\frac{\partial v}{\partial \phi}\right)^2}, \quad \overline{\left(\frac{\partial w}{\partial r}\right)^2}, \quad \overline{\left(\frac{\partial w}{\partial \phi}\right)^2}$$

were not determined directly and are lumped together with the pressure correlations in the remainder term.

For convenience of discussion we adopt the following definitions, with

$$q \equiv \tfrac{1}{2}(\overline{u^2 + v^2 + w^2}).$$

Turbulent energy production:

$$\frac{D}{U_\tau^3}\left[\overline{u^2}\frac{\partial U}{\partial x} + \overline{uv}\left(\frac{\partial V}{\partial x} + \frac{\partial U}{\partial r}\right) + \overline{v^2}\frac{\partial V}{\partial r} + \frac{V\overline{w^2}}{r}\right] \equiv \text{PROD}.$$

Turbulent energy convection:

$$\frac{D}{U_\tau^3}\left[\frac{\partial}{\partial x}(U\overline{q^2}) + \frac{1}{r}\frac{\partial}{\partial r}(rV\overline{q^2})\right] \equiv \text{CONV}.$$

Turbulent energy diffusion:

$$\frac{D}{U_\tau^3}\left[\frac{\partial}{\partial x}\overline{(uq^2)} + \frac{1}{r}\frac{\partial}{\partial r}\overline{(rvq^2)}\right] \equiv \text{DIF}.$$

Gradient diffusion rate of turbulent energy:

$$\frac{D}{U_\tau^3}\left[\frac{\partial^2}{\partial x^2}\overline{q^2} + \frac{1}{r}\frac{\partial}{\partial r}r\frac{\partial}{\partial r}\overline{q^2}\right] \equiv \text{GDIF}.$$

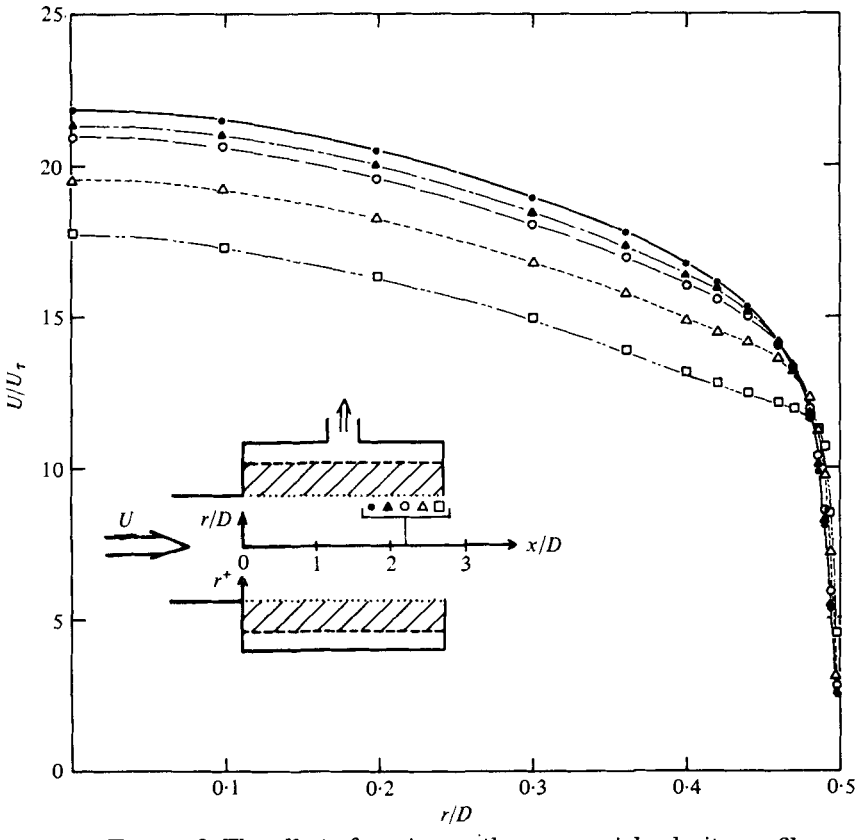

FIGURE 3. The effect of suction on the mean axial velocity profiles ($(Q_A/Q_R) \times 100$): ●, 0; ▲, 1·6; ○, 3·3; △, 6·5; □, 13·0.

Measurable portion of the dissipation:

$$\frac{\nu D}{U_\tau^3}\left[\overline{\left(\frac{\partial u}{\partial x}\right)^2}+\overline{\left(\frac{\partial u}{\partial r}\right)^2}+\overline{\left(\frac{\partial u}{\partial \phi}\right)^2}+\overline{\left(\frac{\partial v}{\partial x}\right)^2}+\overline{\left(\frac{\partial w}{\partial x}\right)^2}\right] \equiv \text{DISM}.$$

Remaining terms, consisting of the turbulent pressure energy diffusion rate and the unmeasured dissipation terms:

$$\frac{\nu D}{U_\tau^3}\left[\overline{\left(\frac{\partial v}{\partial r}\right)^2}+\overline{\left(\frac{\partial w}{\partial r}\right)^2}+\frac{1}{r^2}\overline{\left(\frac{\partial v}{\partial \phi}\right)^2}+\frac{1}{r^2}\overline{\left(\frac{\partial w}{\partial \phi}\right)^2}+\frac{\partial}{\partial x}\left(\overline{\frac{up}{\rho}}\right)+\frac{1}{r}\frac{\partial}{\partial r}\left(r\overline{\frac{vp}{\rho}}\right)\right] \equiv \text{R}.$$

5. Results

The effects of the suction rate

In order to gain insight into the effects of the suction rate on the mean flow and fluctuating quantities, a preliminary investigation was carried out in which extraction rates between 0 and 13 % of the inlet mass flow rate were examined. The mean axial velocity U and the fluctuating components u, v and w were measured at a station half a diameter from the exit plane of the porous-walled section, corresponding to $x/D = 2{\cdot}2$. These results are reported in normalized form in figures 3–6 with Q_A/Q_R,

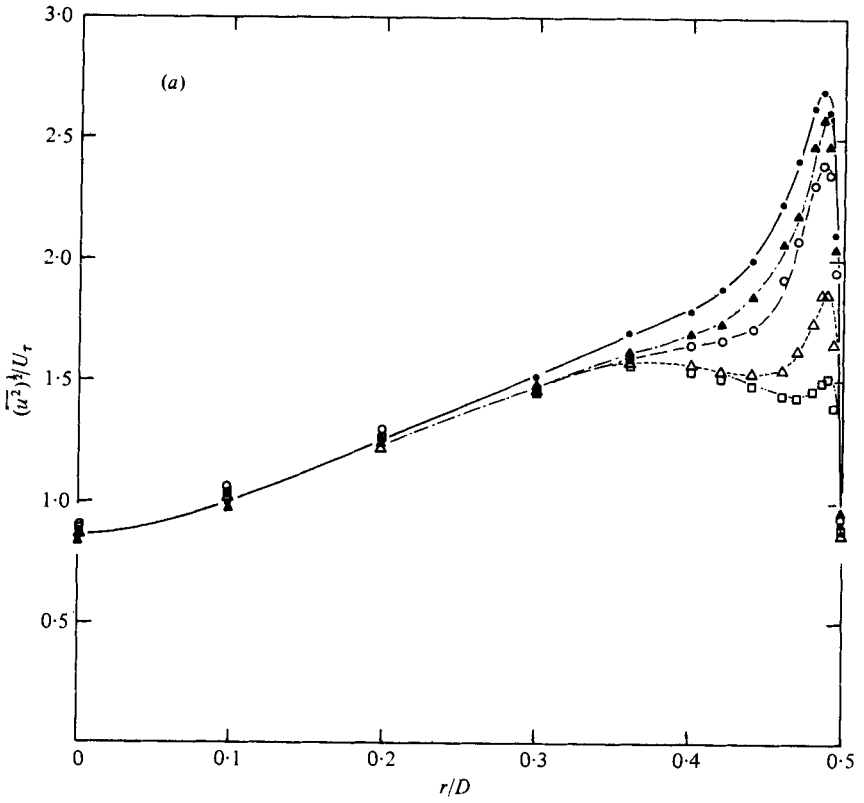
(a)
3·0
2·5
2·0
1·5
1·0
0·5
$(\overline{u^2})^{\frac{1}{2}}/U_\tau$
0
0·1
0·2
0·3
0·4
0·5
r/D

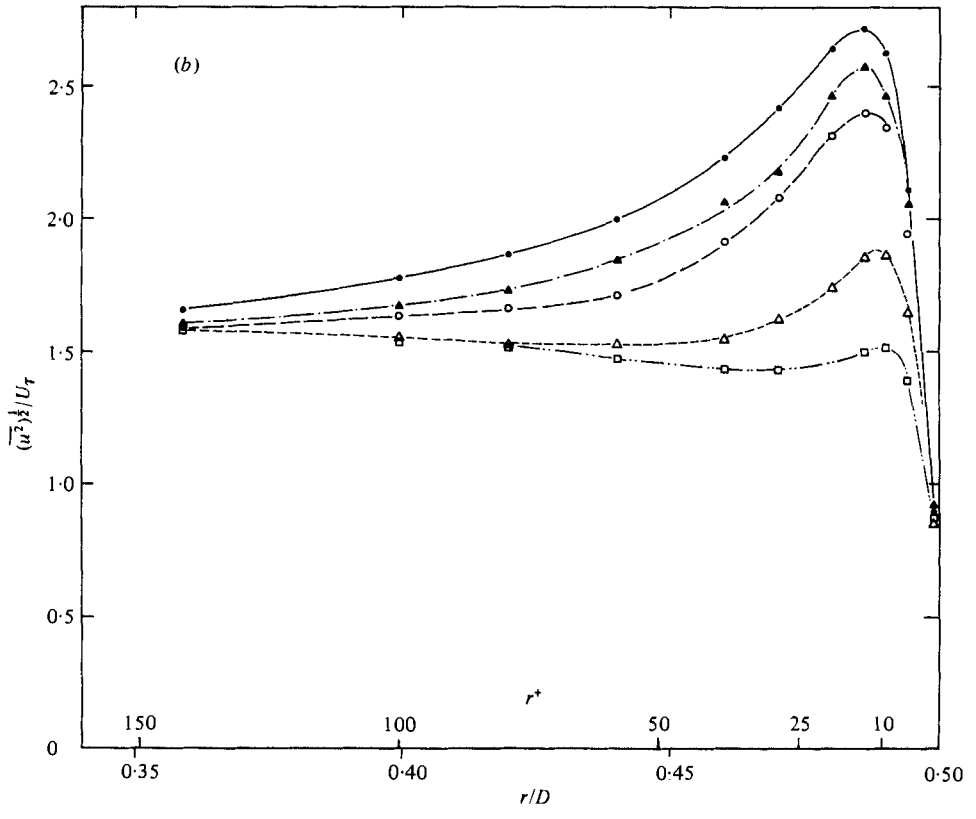
(b)
2·5
2·0
1·5
1·0
0·5
0
$(\overline{u^2})^{\frac{1}{2}}/U_\tau$
r^+
150
100
50
25
10
0·35
0·40
0·45
0·50
r/D

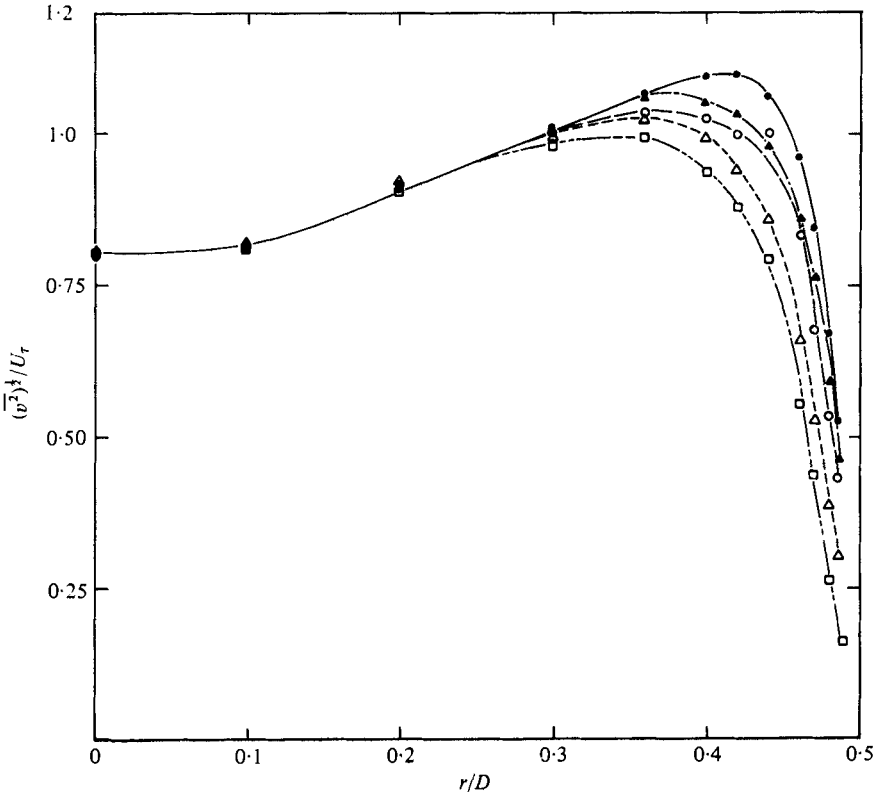

FIGURE 5. The effect of suction on the radial fluctuating velocity profiles. Symbols as in figure 3.

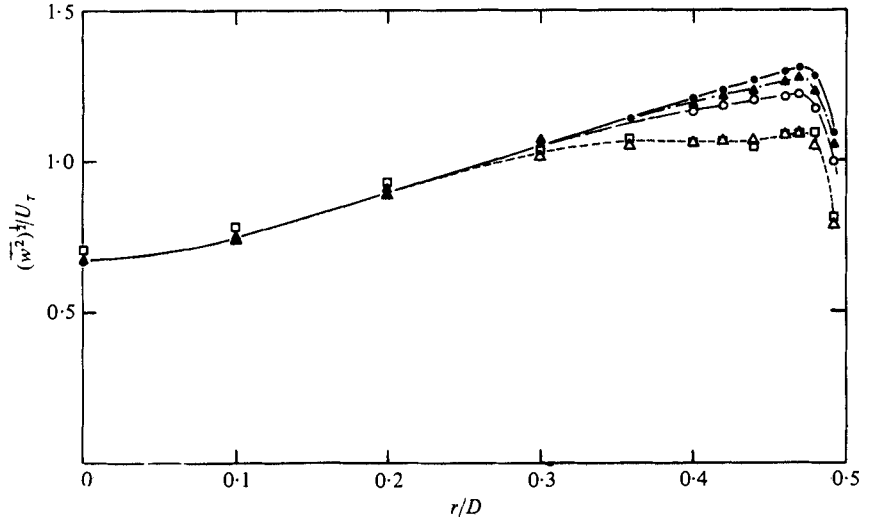

FIGURE 6. The effect of suction on the azimuthal fluctuating velocity profiles. Symbols as in figure 3.

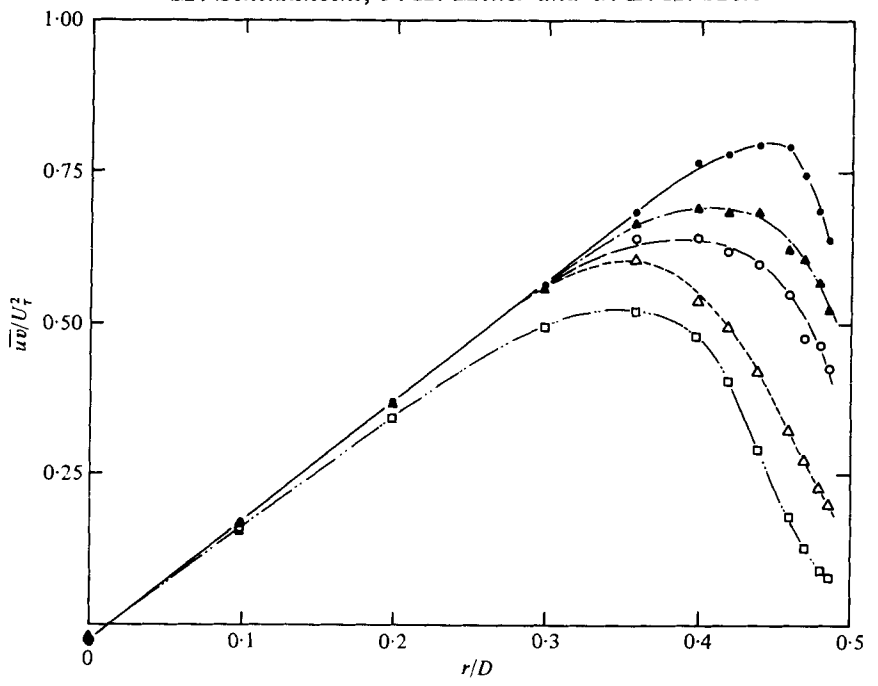

FIGURE 7. The effect of suction on the Reynolds shear stress $\overline{uv}$. Symbols as in figure 3.

the percentage of the inlet mass extracted, as a parameter. As seen in figure 3, these results indicate that increasing mass extraction leads to a more uniform velocity distribution as the wall layers are accelerated and the central flow decelerated by the increasing radial velocity component. There is consequently an increase in the mean molecular shear stress near the wall, implying an associated increase in the dissipation of the mean flow. At the largest two extraction rates investigated an inflexion was produced in the mean velocity profile at $r/D \cong 0{\cdot}4$.

The effects of suction on the fluctuating velocity components may be seen in figures 4–6. These results indicate a general reduction in the absolute level of fluctuation intensity with increasing wall suction as reported previously by Weissberg & Bergman (1955), among others. Moreover there appear to be only minor migrations in the location of the maxima in the fluctuation distributions, which leads to the belief that the location of these maxima is a relatively stable property of turbulent flows.

It is also apparent from these results that the effect of suction does not propagate into the entire flow immediately and that the propagation rate is only a weak function of the suction rate.

From figures 5 and 6 one sees that the effects of suction on turbulent structure cannot be interpreted as a single convective effect, i.e. the turbulent state of the fluid is not simply convected to a new location by the increasing radial velocity component.

The normalized Reynolds stress, reported in figure 7, shows that there is a pronounced reduction in this momentum-transfer quantity in the wall layers even for very small suction rates. On comparing these results with the alteration in the mean velocity profiles reported in figure 3, one concludes that the effect of wall suction is to reduce markedly the domain in which the Reynolds stress is small with respect to the mean molecular stress.

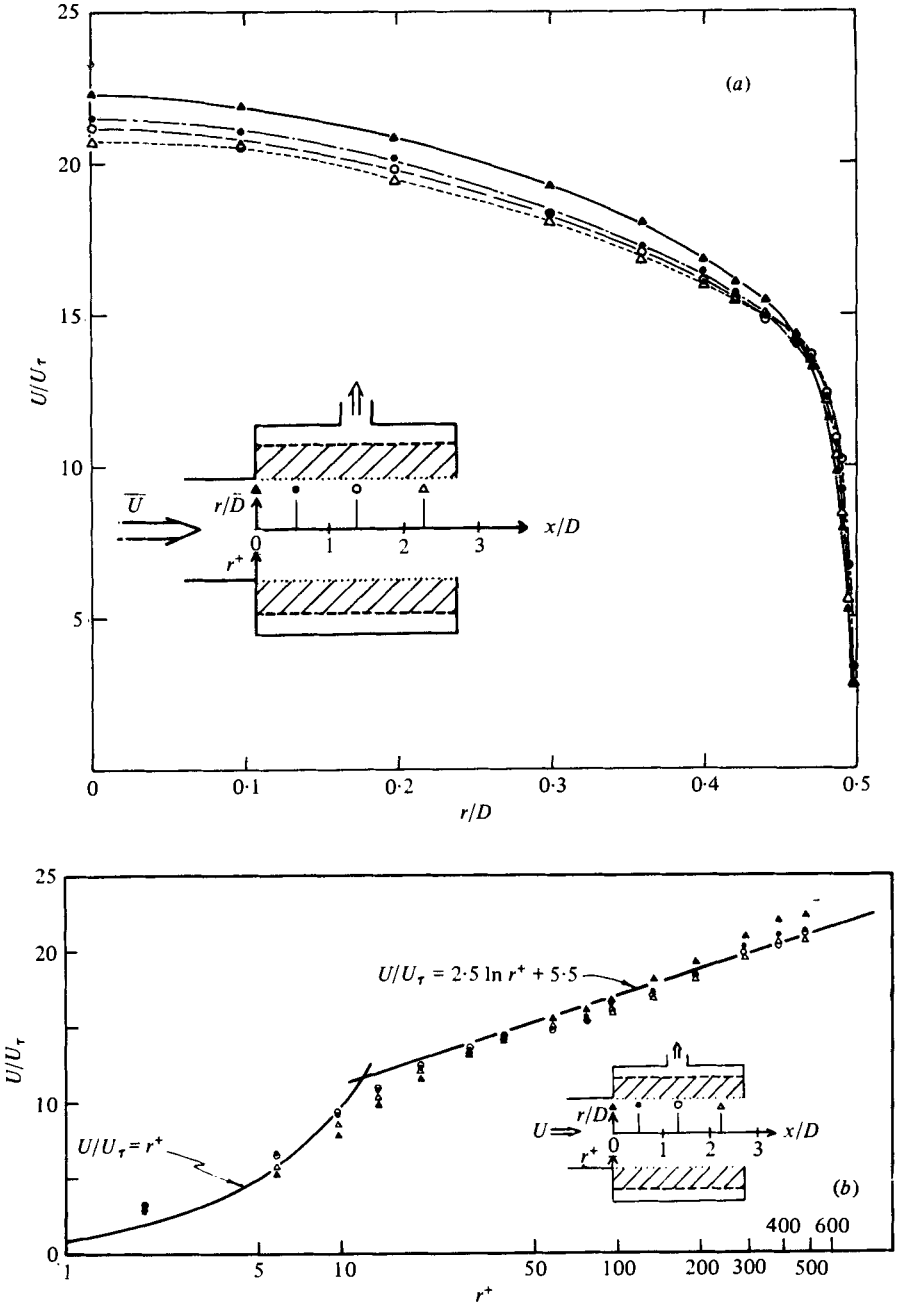

FIGURE 8. Mean axial velocity profiles. (*b*) shows the wall layer on a larger scale. x/D: ▲, 0; ●, 0·503; ○, 1·358; △, 2·213.

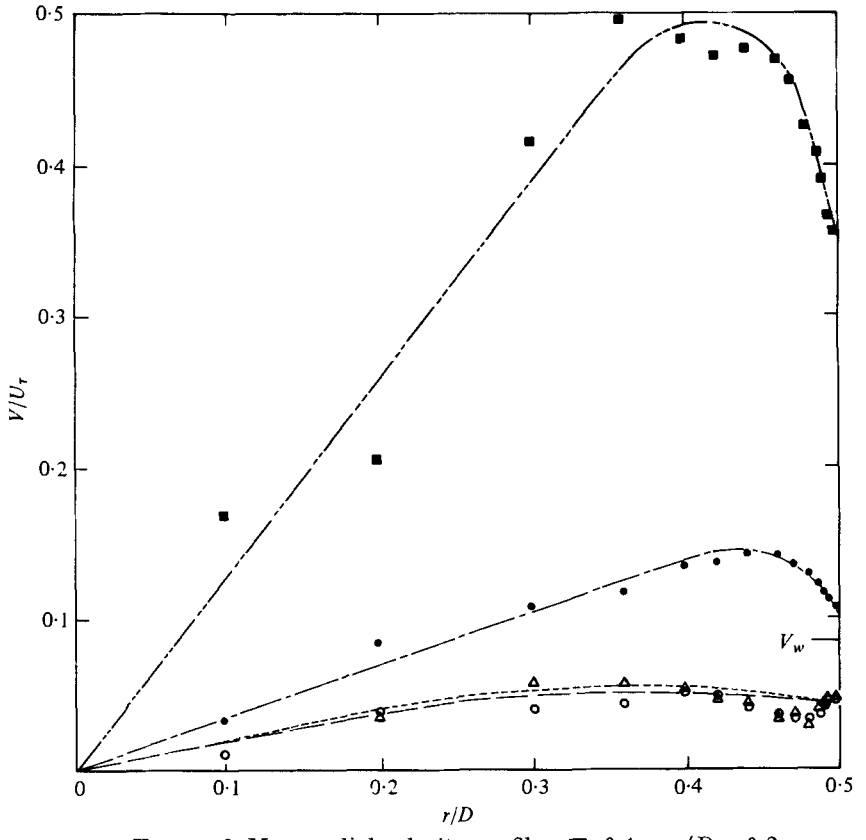

FIGURE 9. Mean radial velocity profiles. ■, $0{\cdot}1 < x/D < 0{\cdot}2$; other symbols as in figure 8.

The effects of a small suction rate

In an attempt to retain the essential character of a fully developed pipe flow, a suction rate of about 4 % of the mean mass flow rate was adopted for the balance of the study. From the preliminary results this suction rate may be expected to produce a significant (and measurable) perturbation in the fluctuating amplitudes while leaving the mean velocity profile little altered. The resulting mass extraction reduces the Reynolds number through the test section by about 4 % from a value of 17250 in the fully developed flow at the entrance plane $x/D = 0$ to 16550 at the exit plane $x/D = 2{\cdot}2$. Measurements were made at four axial stations corresponding to $x/D = 0$, 0·5, 1·4 and 2·2, the results at $x/D = 0$ corresponding to a fully developed turbulent pipe flow.

The mean axial velocities are reported in figure 8, from which it is evident that the small rate of suction produces no major modification of the profile.

Because the mean radial velocity V was very small, it could not be measured with adequate accuracy with a cross-wire probe and was calculated from the measured values of the axial velocity and the continuity equation:

$$V(r,x) = \frac{1}{r}\int_0^r -r\frac{\partial U(r,x)}{\partial x}\,dr.$$

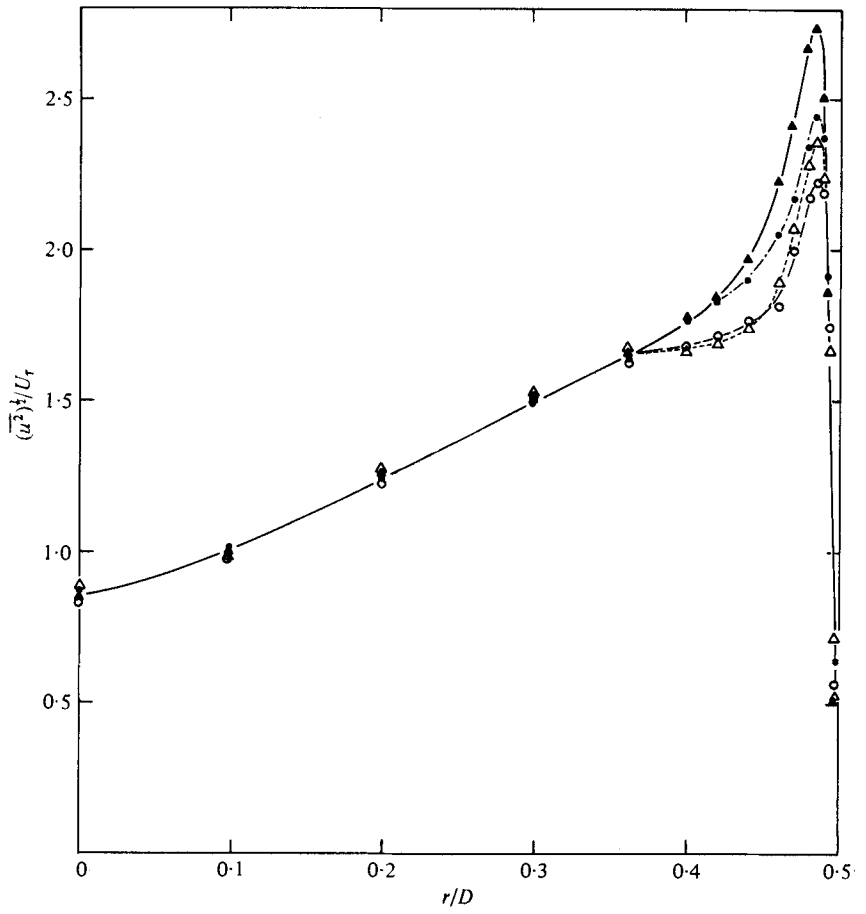

FIGURE 10. Distribution of axial fluctuating velocity component. Symbols as in figure 8.

The results are shown in figure 9. From these results one sees that a high rate of fluid extraction prevails close to the entrance plane and relaxes to a fully developed state at about $x/D = 1{\cdot}3$. The symbol V_w denotes the value of the radial velocity at the wall calculated from the measured extraction rate under the assumption of uniform suction along the test section.

Since the mean radial velocity distribution should depend only on the construction of the porous test section, we may reasonably assume that the axial distribution reported in figure 9 for a suction rate of 4 % is representative of a wide range of suction rates.

The mean values $\overline{u^2}$, $\overline{v^2}$, $\overline{w^2}$ and $\overline{uv}$ of the fluctuation components are shown in figures 10–13. These results demonstrate that the effects of suction propagate inwards from the wall, penetrating to about $r/D = 0{\cdot}3$ at the exit plane of the porous section $x/D = 2{\cdot}2$. Using the quantity $\overline{u^3}$, reported in figure 14, as a criterion because of its sensitivity, the location of the departure from its value in fully developed flow has been plotted in figure 15. From this plot the radial propagation velocity of the influence of wall suction has been determined to be $U_{ti} = 0{\cdot}3\,\mathrm{m/s}$, which is almost identical to the friction velocity $U_\tau = 0{\cdot}29\,\mathrm{m/s}$.

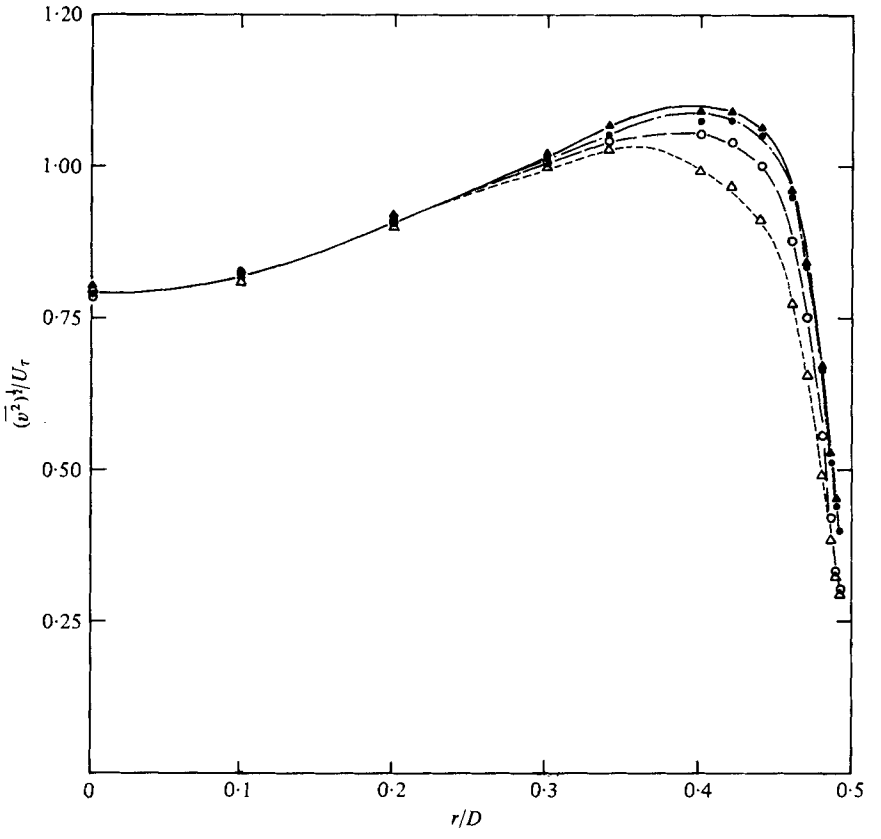

FIGURE 11. Distribution of radial fluctuating velocity component. Symbols as in figure 8.

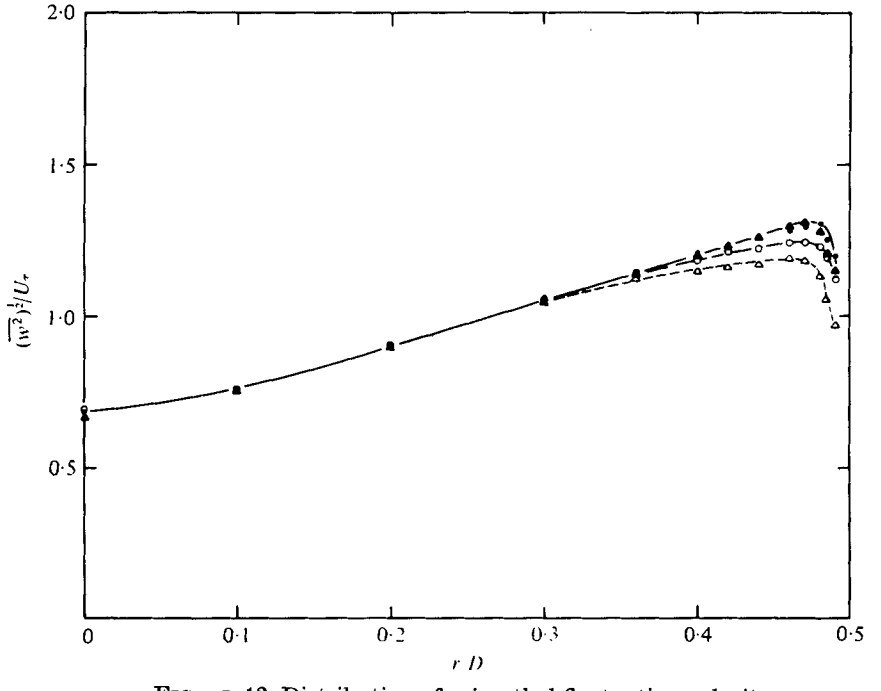

FIGURE 12. Distribution of azimuthal fluctuating velocity component. Symbols as in figure 8.

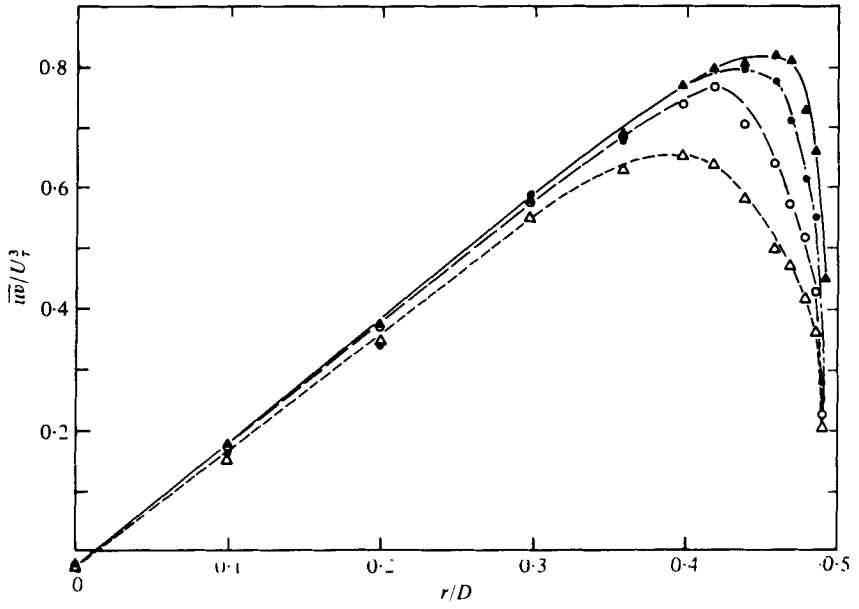

FIGURE 13. Distribution of the Reynolds stress $\overline{uv}$. Symbols as in figure 8.

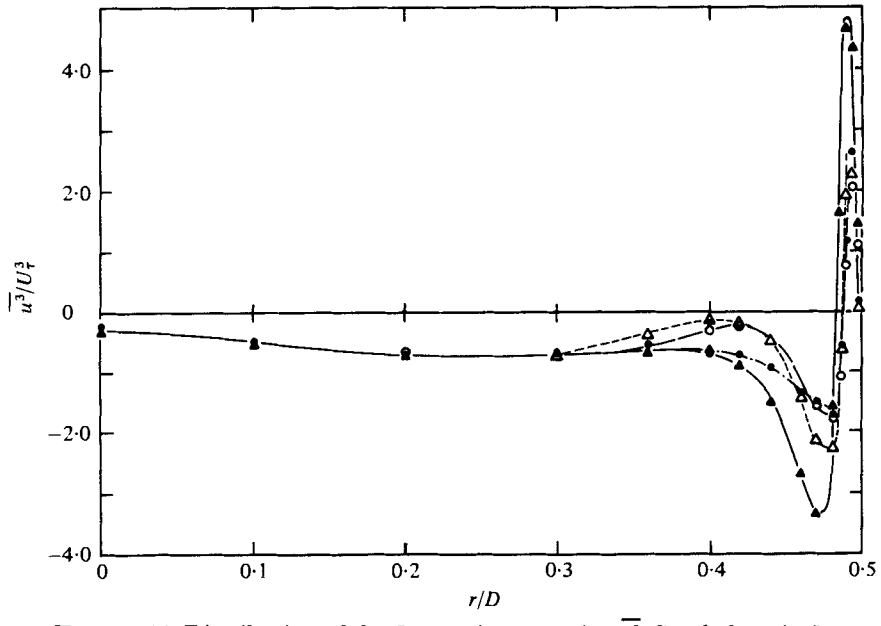

FIGURE 14. Distribution of the fluctuation quantity $\overline{u^3}$. Symbols as in figure 8.

In figure 16 data for $\overline{u^2}$, $\overline{v^2}$, $\overline{w^2}$ and $\overline{uv}$ for the wall layers are plotted as well as the data of Laufer (1953), Eckelmann (1974) and Kreplin (1976). The last two authors made measurements in an oil channel which produced very thick viscous layers leading to a high order of accuracy. The present results are in excellent agreement with those of these other workers except in the case of $\overline{w^2}$, where the present

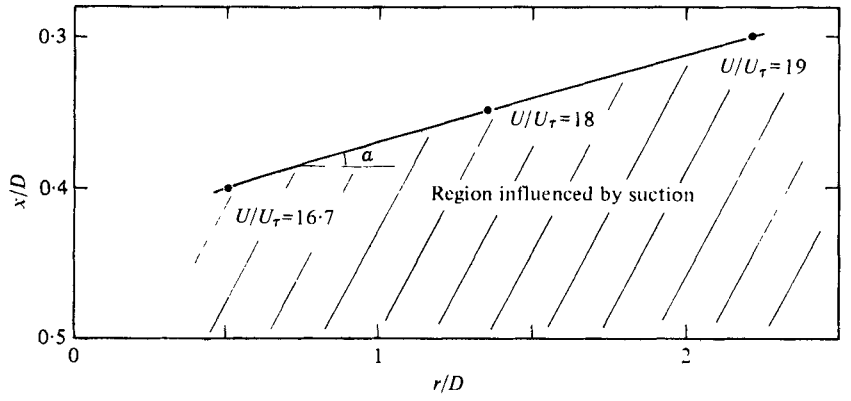

FIGURE 15. Radial propagation of the effects of wall suction. $U_{tt} = 0{\cdot}3\,\mathrm{m/s} \approx U_\tau$.

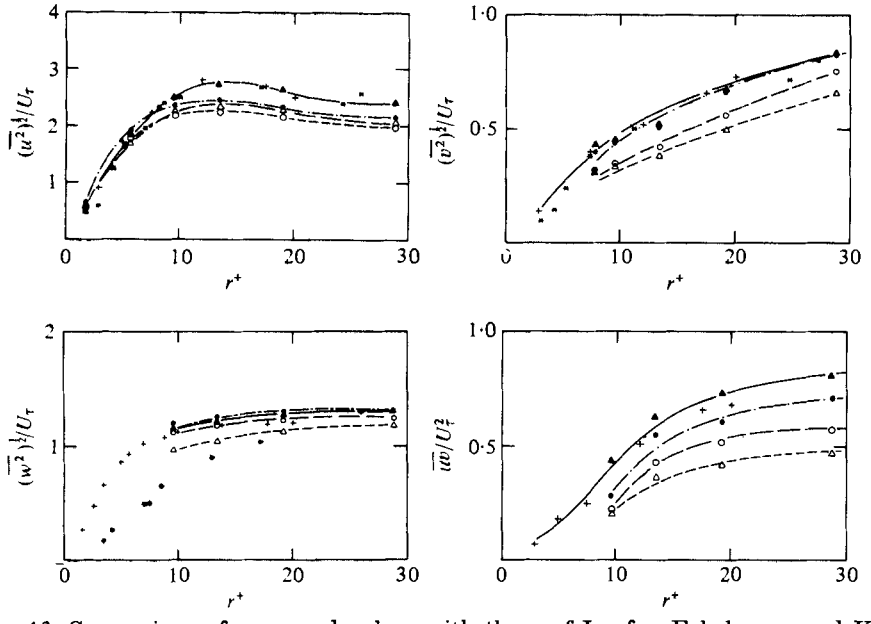

FIGURE 16. Comparison of measured values with those of Laufer, Eckelmann and Kreplin in the wall layer. +, Eckelmann (1974), Kreplin (1976); *, Laufer (1953); other symbols as in figure 8.

measurements as well as those of Eckelmann and Kreplin are substantially larger than those reported earlier by Laufer.

The remaining principal third-order moments,

$$\frac{\overline{uv^2}}{U_\tau^3}, \quad \frac{\overline{uw^2}}{U_\tau^3}, \quad \frac{\overline{v^3}}{U_\tau^3}, \quad \frac{\overline{u^2v}}{U_\tau^3}, \quad \frac{\overline{vw^2}}{U_\tau^3},$$

are reported in figures 17–21. The principal spatial gradients of the fluctuating components,

$$\frac{\nu D}{U_\tau^3}\left(\overline{\frac{\partial u}{\partial r}}\right)^2, \quad \frac{\nu D}{U_\tau^3}\frac{1}{r^2}\left(\overline{\frac{\partial u}{\partial \phi}}\right)^2, \quad \frac{\nu D}{U_\tau^3}\left(\overline{\frac{\partial v}{\partial x}}\right)^2, \quad \frac{\nu D}{U_\tau^3}\left(\overline{\frac{\partial w}{\partial x}}\right)^2,$$

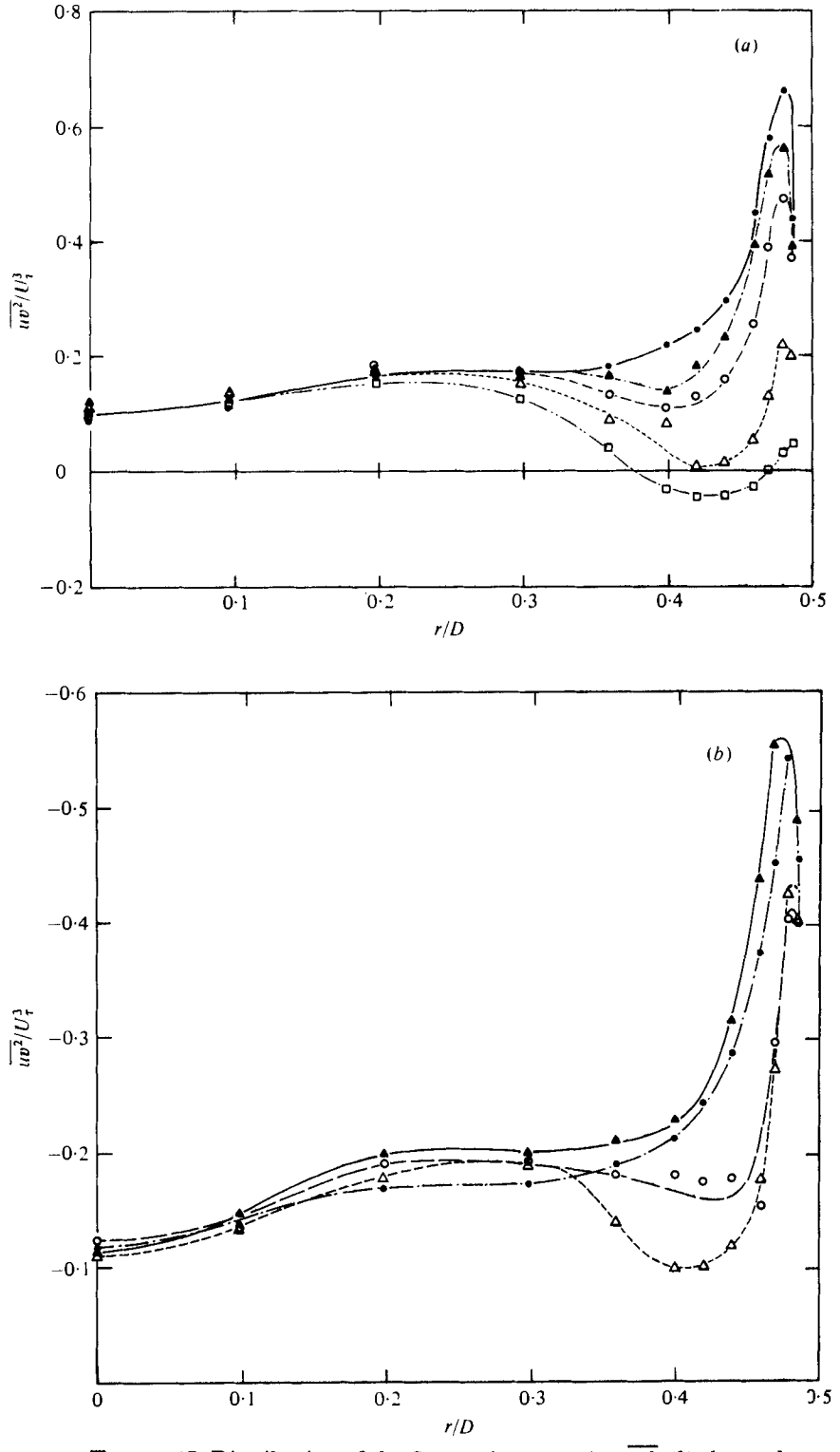

FIGURE 17. Distribution of the fluctuation quantity $\overline{uv^2}$. (*b*) shows the wall layer on a larger scale. Symbols as in figure 8.

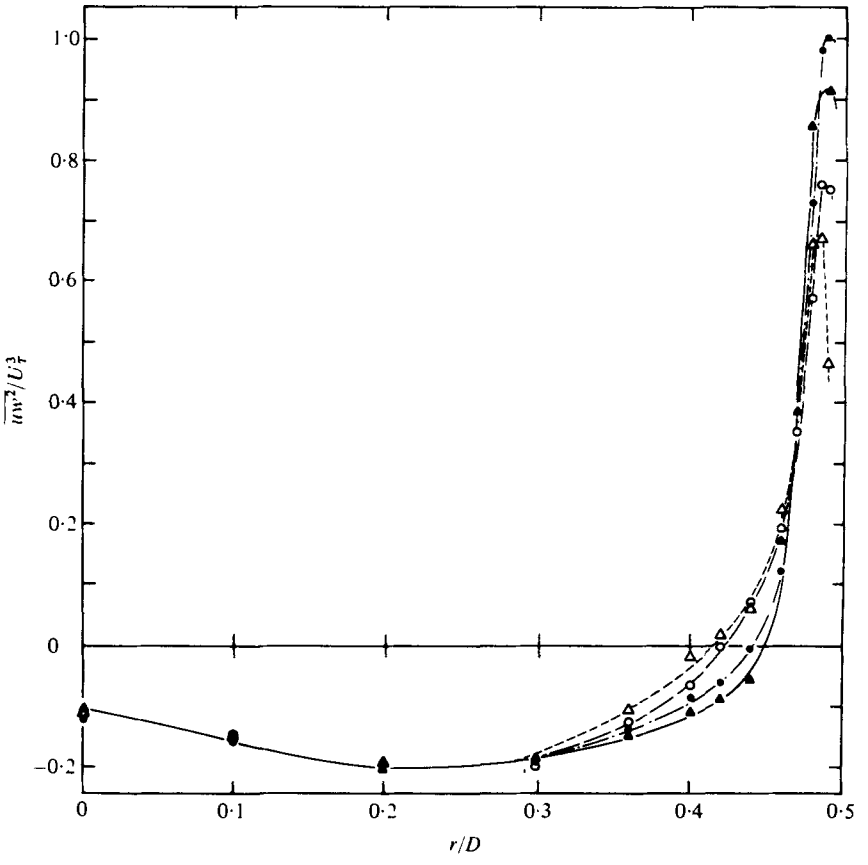

FIGURE 18. Distribution of the fluctuation quantity $\overline{uw^2}$. Symbols as in figure 8.

are shown in figures 22–25. In all of these data the values reported for $x/D = 0$ represent data in a fully developed turbulent pipe flow without wall suction.

Behaviour of the individual components of the energy balance

The measured rate of turbulent energy production PROD is reported in figure 26 and the behaviour of the term $(\partial U/\partial r)\overline{uv}$, which represents the rate of turbulent energy production in a flow without suction, is shown in figure 27. One sees that the production of turbulent energy vanishes both at the centre-line and at the wall in accordance with the boundary conditions discussed above. Moreover it is apparent that the quantity $(\partial U/\partial r)\overline{uv}$ is the dominant term in the turbulent energy production term. Suction effects a dramatic reduction in turbulent energy production, by as much as 50% in the wall layers, and this reduction is traceable almost entirely to the reduction in the Reynolds stress $\overline{uv}$ along the suction section. The gradient of the mean velocity $\partial U/\partial r$, whose values near the wall are somewhat increased with increasing radial mean velocity at the wall, as shown in figure 8, shows only a slight change in comparison with the reduction in $\overline{uv}$.

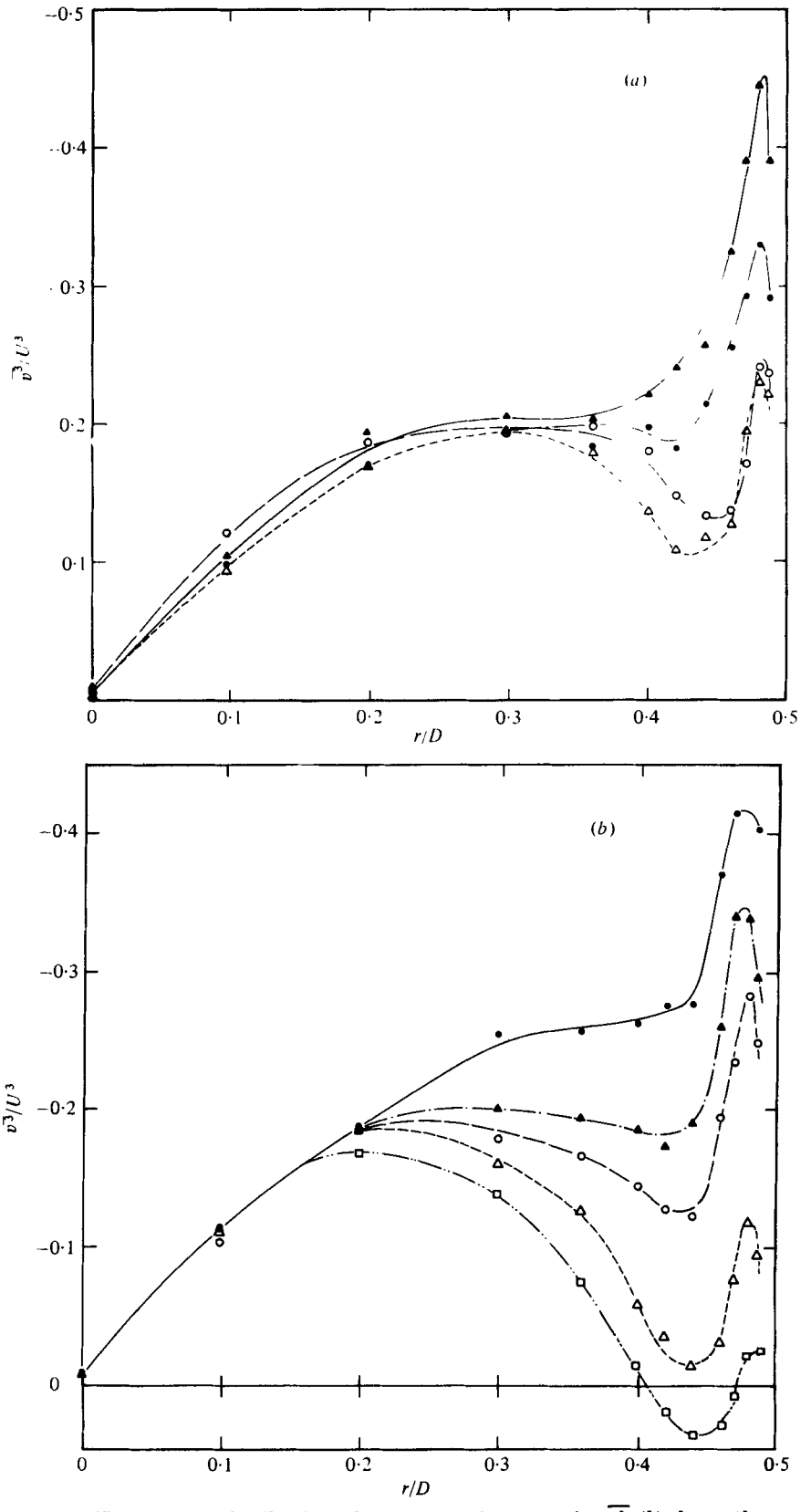

FIGURE 19. Distribution of the fluctuation quantity $\overline{v^3}$. (*b*) shows the wall layer on a larger scale. Symbols as in figure 8.

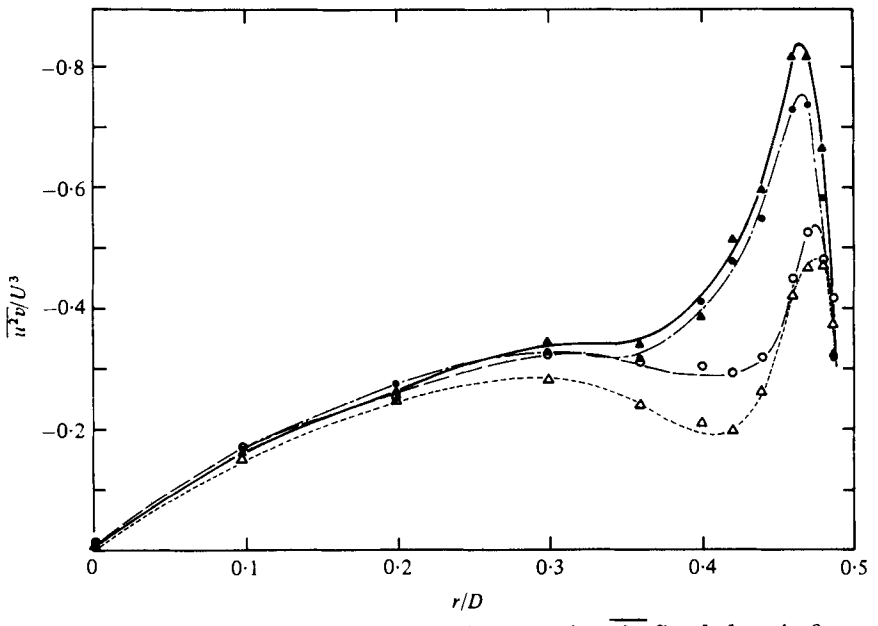

FIGURE 20. Distribution of the fluctuation quantity $\overline{u^2v}$. Symbols as in figure 8.

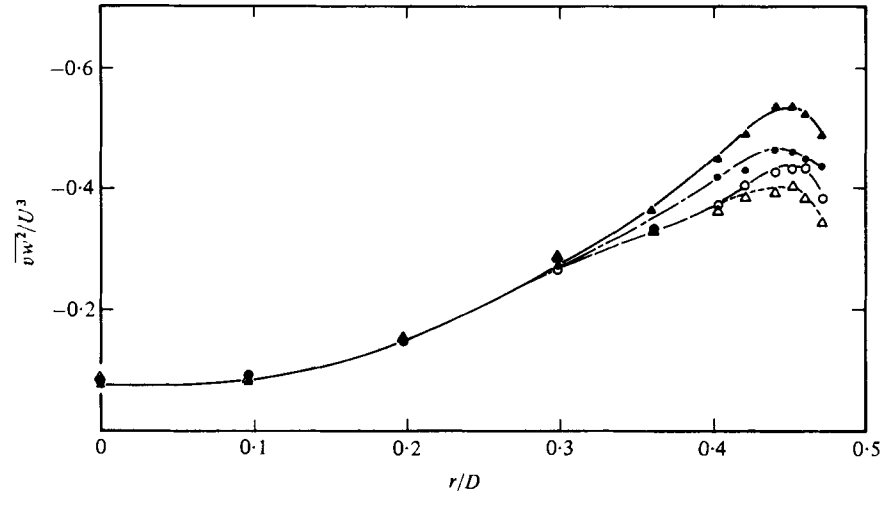

FIGURE 21. Distribution of the fluctuation quantity $\overline{vw^2}$. Symbols as in figure 8.

The introduction of a mean radial velocity in fully developed flow leads to the formation of the additional terms $\overline{v^2}\,\partial U/\partial r$, $\overline{u^2}\,\partial U/\partial x$, $\overline{uv}\,\partial V/\partial x$ and $V\overline{w^2}/r$ in the production term. The first of these tends to increase the rate of production of turbulent energy in the wall layers while the second tends to reduce it. At greater distances from the wall, corresponding to the radial location where $\partial V/\partial r$ vanishes, the effects of these two terms become reversed. Except perhaps in the interval $0{\cdot}1 < x/D < 0{\cdot}2$, where $V(r, x)$ has a maximum, the third additional term is small and may be neglected

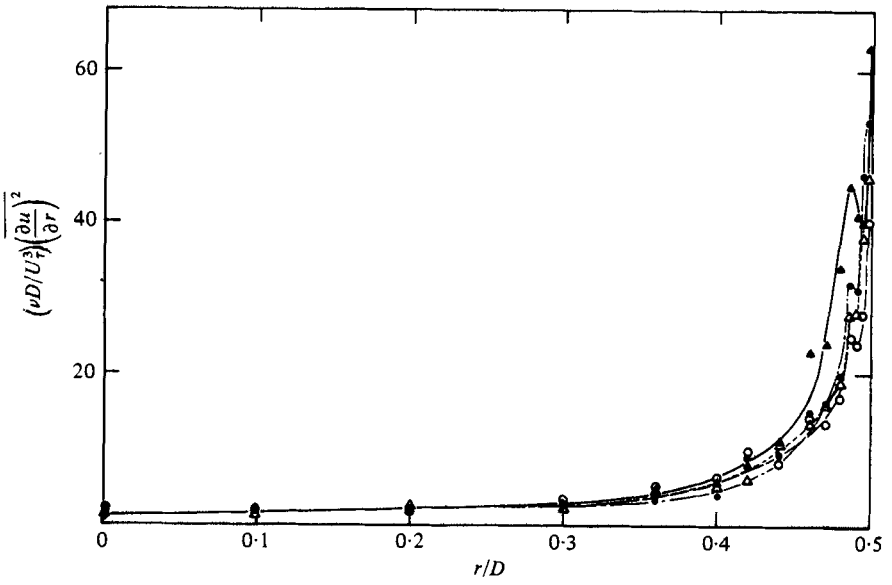

FIGURE 22. Distribution of $\overline{(\partial u/\partial r)^2}$. Symbols as in figure 8.

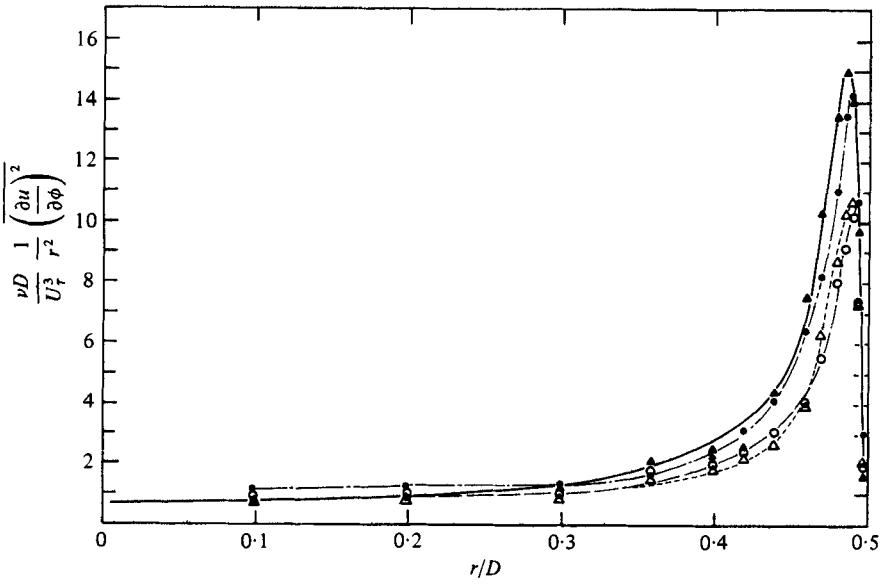

FIGURE 23. Distribution of $\overline{(\partial u/\partial \phi)^2}$. Symbols as in figure 8.

since $\partial U/\partial x$ is small, from continuity. The last additional term is everywhere small with respect to the remaining terms as demonstrated by the measurements. A comparison of figures 26 and 27 demonstrates that all the additional production terms may be neglected for $x/D > 1{\cdot}3$.

Figure 28 reports the distribution of turbulent energy convection due to the alteration in the mean motion. These terms are of course not present in a fully developed flow. Because of the wall boundary condition discussed above, one expects this term

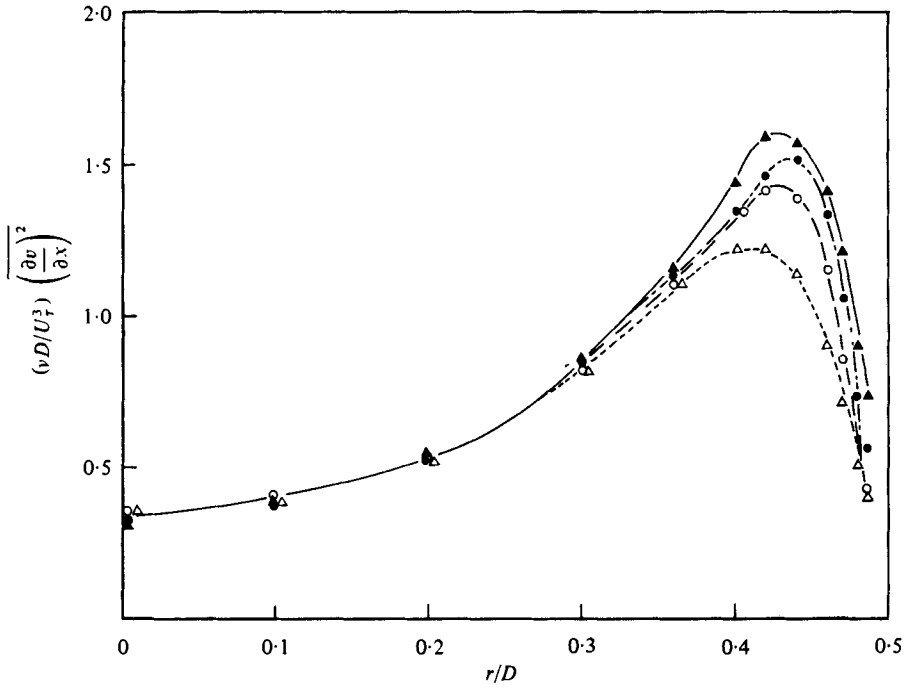

FIGURE 24. Distribution of $\overline{(\partial v/\partial x)^2}$. Symbols as in figure 8.

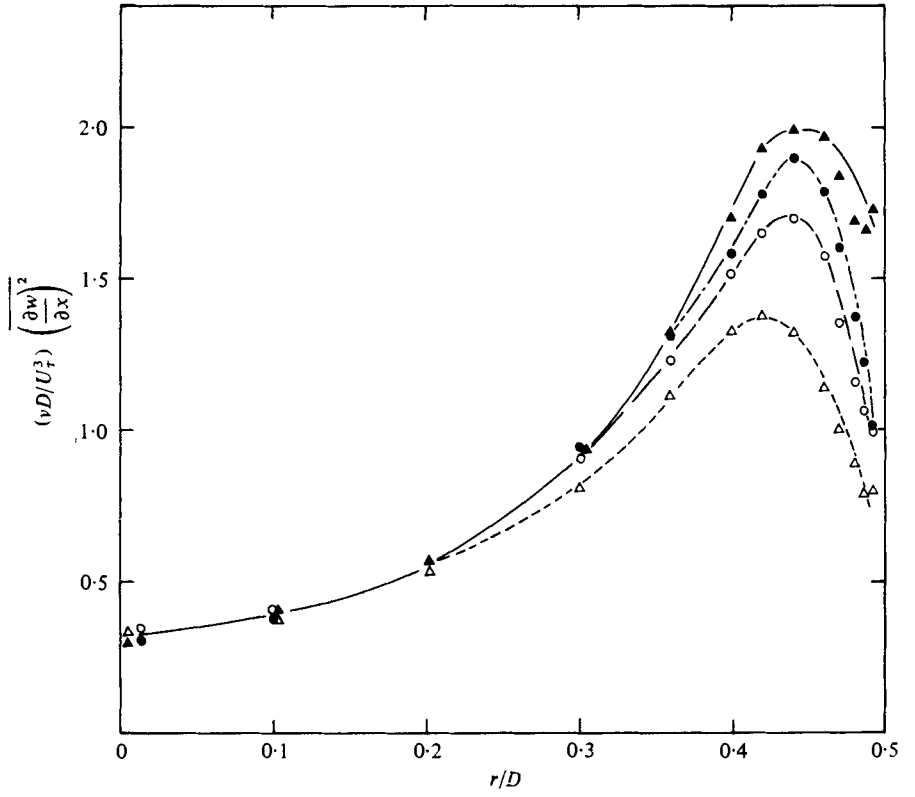

FIGURE 25. Distribution of $\overline{(\partial w/\partial x)^2}$. Symbols as in figure 8.

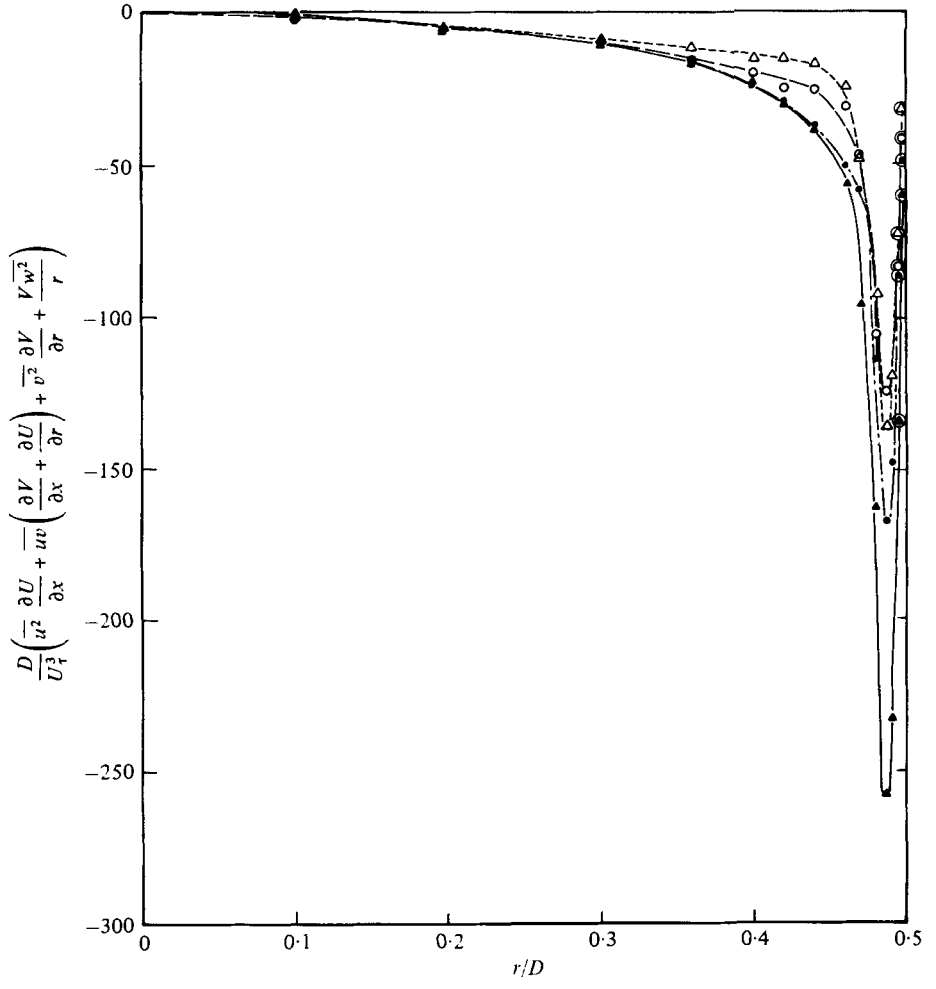

FIGURE 26 (*a*). For legend see next page.

to vanish at the wall, and if one assumes that $\partial q/\partial x$ and $\partial q/\partial r$ vanish at the centre-line (the measurements support this assumption), then this term should also vanish on the centre-line. A detailed examination of the measurements reveals that the dominant quantity in the wall layers is the product $V\partial q/\partial r$, which is an order of magnitude greater than the remaining components. In a flow with suction the gradient of the turbulent kinetic energy near the wall depends principally on the mechanical structure of the porous wall. High gradients result when the holes are small as this inhibits fluctuations at the wall as discussed above. For larger holes the turbulent kinetic energy may be carried through the porous wall and need not vanish at the wall. In such a case the convection term would be smaller in the wall layers and remain finite at the wall itself. The large differences in the values of the maxima reported in figure 28(*b*) are traceable almost entirely to the streamwise variation in the radial mean velocity. In the core of the flow both parts of the convective term assume equal values and opposite signs and vanish. Near the wall the convective term has the same sign

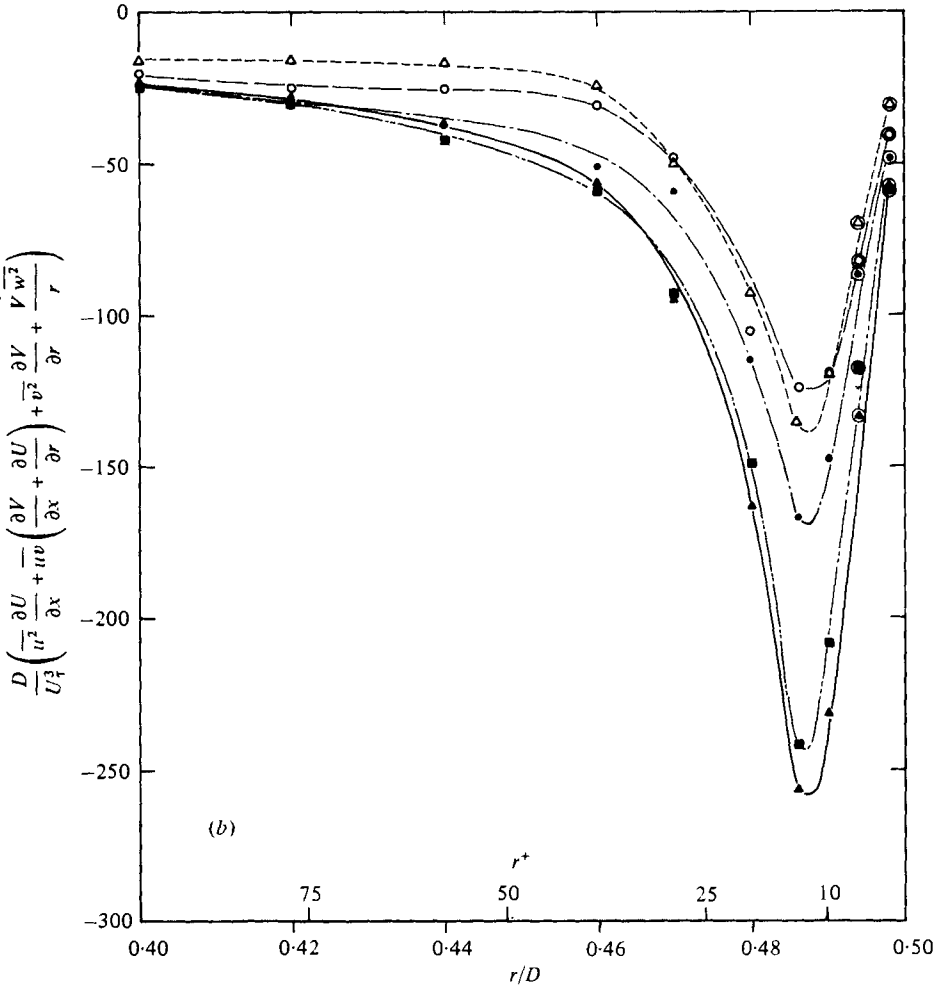

FIGURE 26. Turbulent energy production. (*b*) shows the wall layer on a larger scale. --■--, $0{\cdot}1 < x/D < 0{\cdot}2$; other symbols as in figure 8.

as the production term and is, near the entrance section, roughly equal in magnitude to the production term.

The distribution of turbulent energy convection due to the fluctuating motion is reported in figure 29. Because of the boundary condition that inhibits fluctuations at the wall this term must also vanish at the wall; however it may have finite values on the pipe centre-line. The term containing r-wise derivatives, which represents the entire convection due to fluctuating motion in a fully established flow without suction, is everywhere at least one order of magnitude greater than the additional terms occasioned by the presence of wall suction. These additional terms tend to decrease the total quantity for $x/D < 1{\cdot}3$ and increase it for greater values of x/D.

The gradient diffusion rate of turbulent energy GDIF is reported in figure 30 for the wall layers, the only region in which it is non-negligible. The term containing the x-wise derivatives is two orders of magnitude smaller than the balance of the quantity

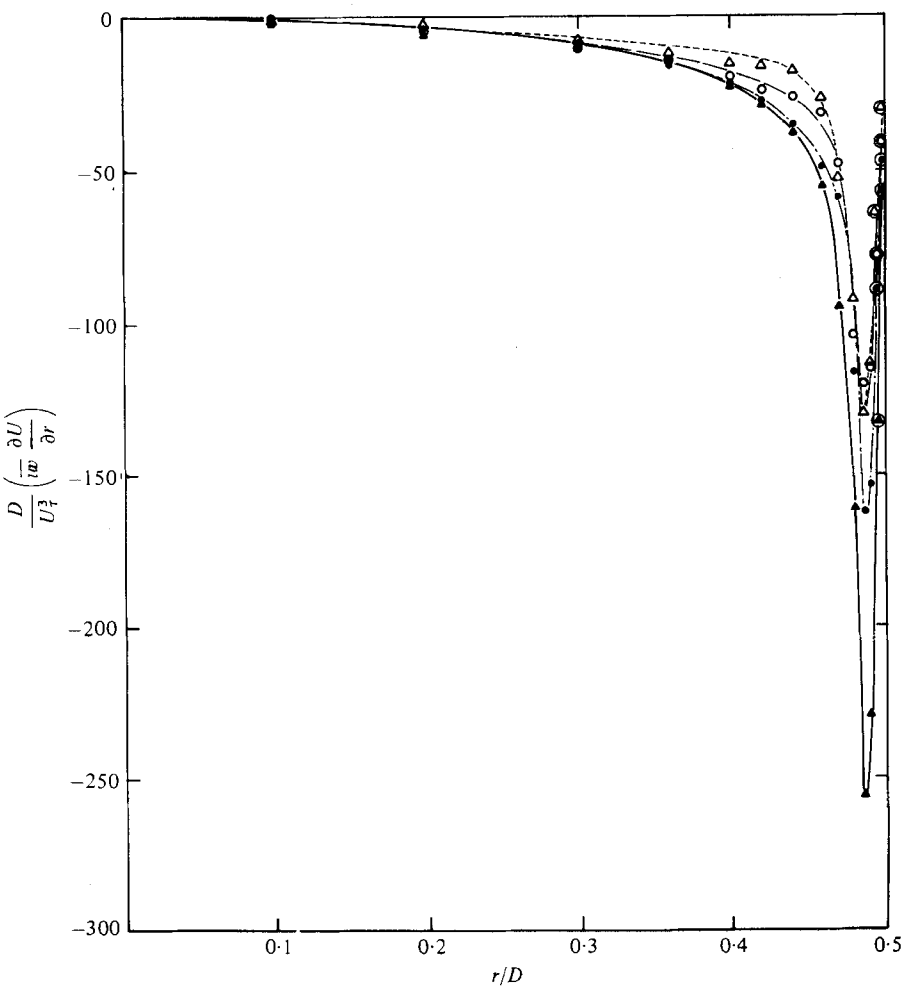

FIGURE 27 (*a*). For legend see next page.

and does not contribute significantly. Because of the boundary conditions discussed above, the gradient diffusion rate must vanish along the pipe centre-line but may remain finite at the wall. Very close to the wall the fluctuating quantities tend to be linear in r and the gradient diffusion term tends to a constant value. Because this term is significant only in the wall layers it becomes fully developed very quickly in the axial direction, in about a single diameter.

Figure 31 reports the distribution of the principal components of the dissipation term, $\overline{(\partial u/\partial x)^2}$, $\overline{(\partial u/\partial r)^2}$ and $\overline{(\partial u/\partial \phi)^2}$, at the entrance plane of the porous wall section. Of these, only $\overline{(\partial u/\partial r)^2}$ is expected to be non-zero at the wall. Along the pipe centre-line one expects these quantities to remain finite and, because of isotropy, equal. The measurements confirm this.

The effect of suction on the quantity $\overline{(\partial u/\partial x)^2}$ is shown in figure 32 and is seen to be confined to the wall layers. The results for $\overline{(\partial v/\partial x)^2}$ and $\overline{(\partial w/\partial x)^2}$ are qualitatively similar but about 30 % smaller in absolute magnitude.

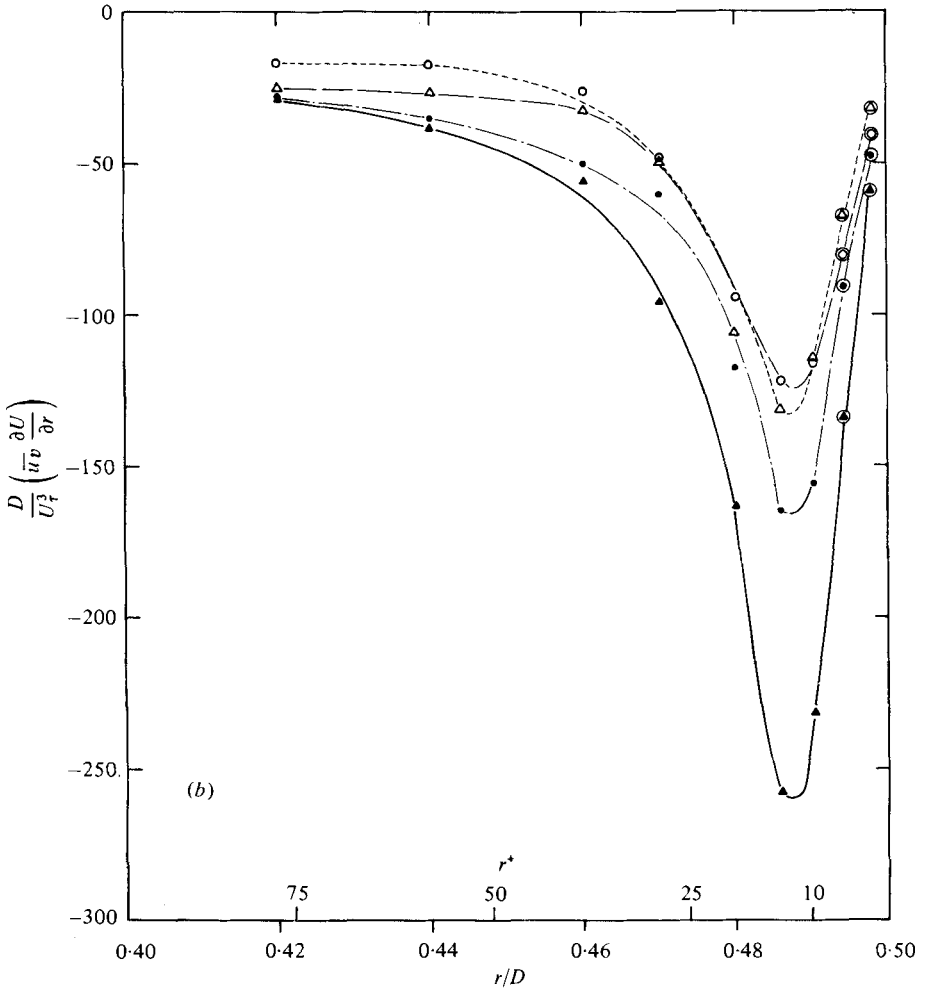

FIGURE 27. Distribution of $\overline{uv}\,\partial U/\partial r$. (*b*) shows the wall layer on a larger scale. Symbols as in figure 8.

The largest single contribution to the dissipation term is attributable to the quantity $\overline{(\partial u/\partial r)^2}$, whose distribution is shown in figure 33(*a*). The local maximum in this quantity appearing at about $r/D = 0{\cdot}485$ corresponds to the maximum in the measured distribution of $\overline{u^2}$. The point denoted by D_w corresponds to the value of $\overline{(\partial u/\partial r)^2}$ at the wall obtained by Eckelmann (1974) by use of a flush-mounted hot-film wall gauge. Note that this term is not as strongly quenched by wall suction as is the production term in the wall layers.

The effect of suction on $\overline{(\partial u/\partial \phi)^2}$ is shown in figure 33(*b*). This effect, which is confined to the wall layers, becomes fully developed in approximately one diameter.

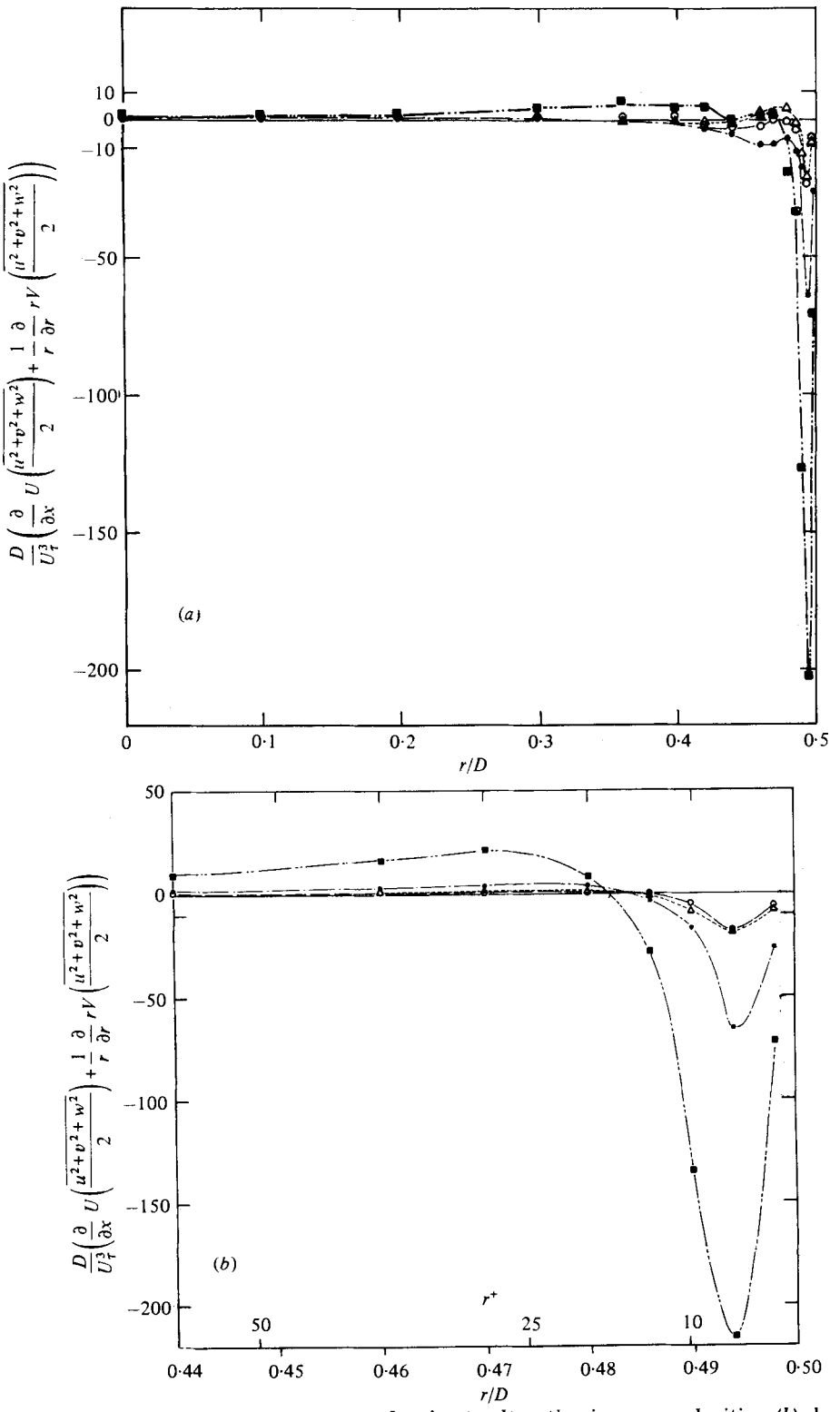

FIGURE 28. Turbulent energy convected owing to alteration in mean velocities. (*b*) shows the wall layer on a larger scale. --■--, $0{\cdot}1 < x/D < 0{\cdot}2$; other symbols as in figure 8.

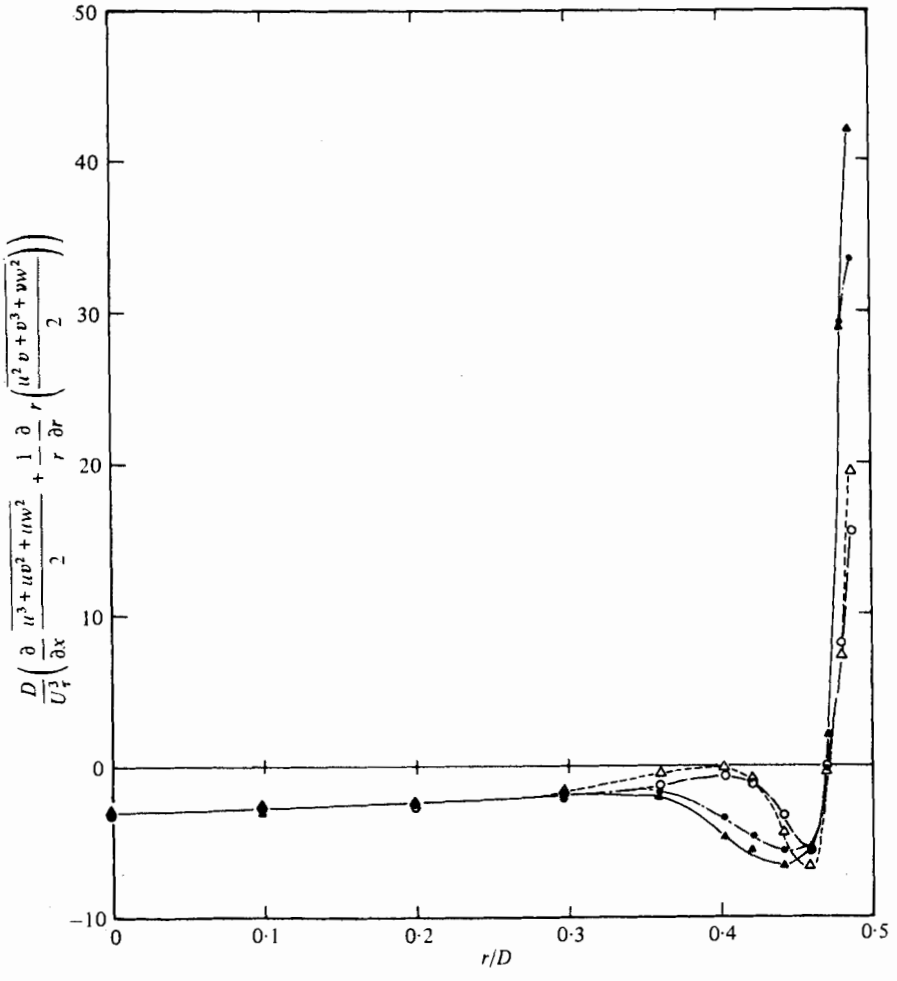

FIGURE 29(*a*). For legend see facing page.

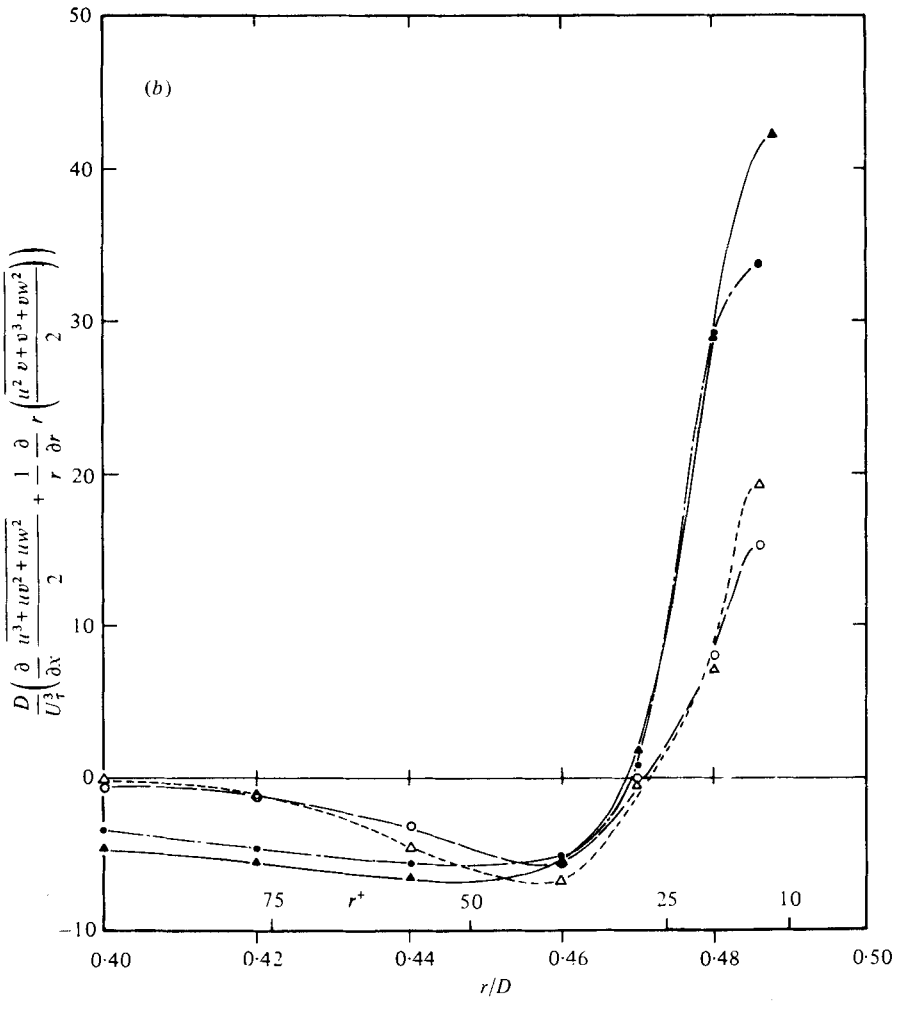

FIGURE 29. Turbulent energy convected owing to the fluctuating velocities. (*b*) shows the wall layer on a larger scale. Symbols as in figure 8.

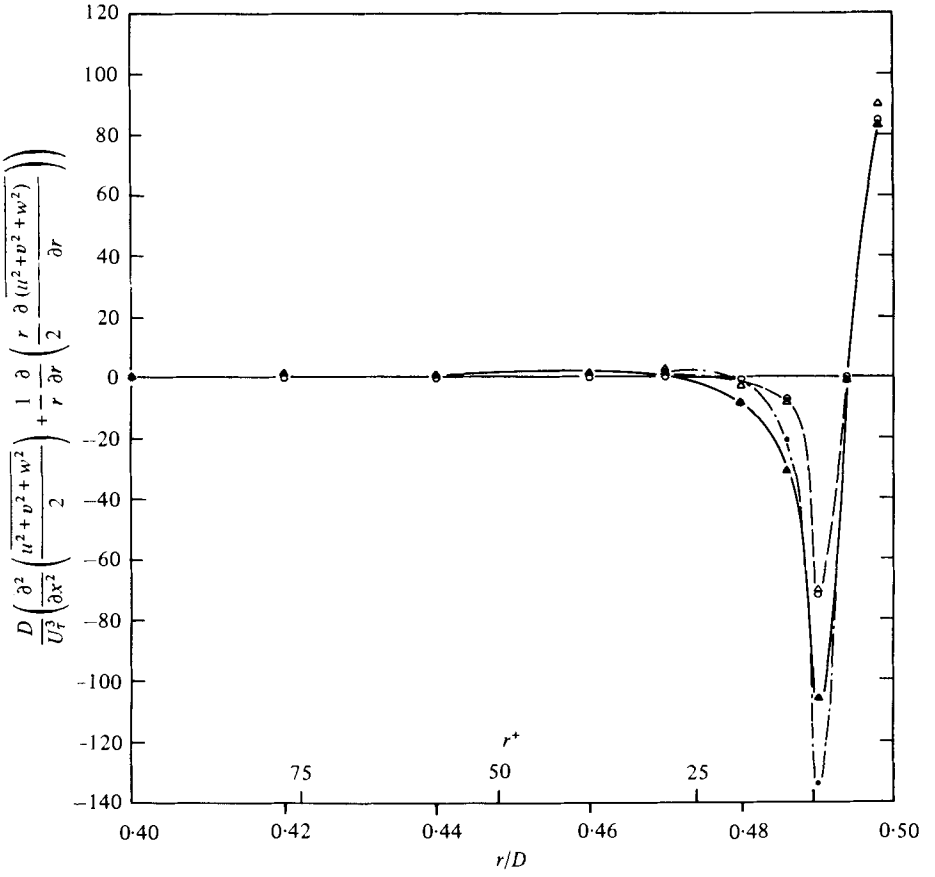

FIGURE 30. The gradient diffusion rate of turbulent energy. Symbols as in figure 8.

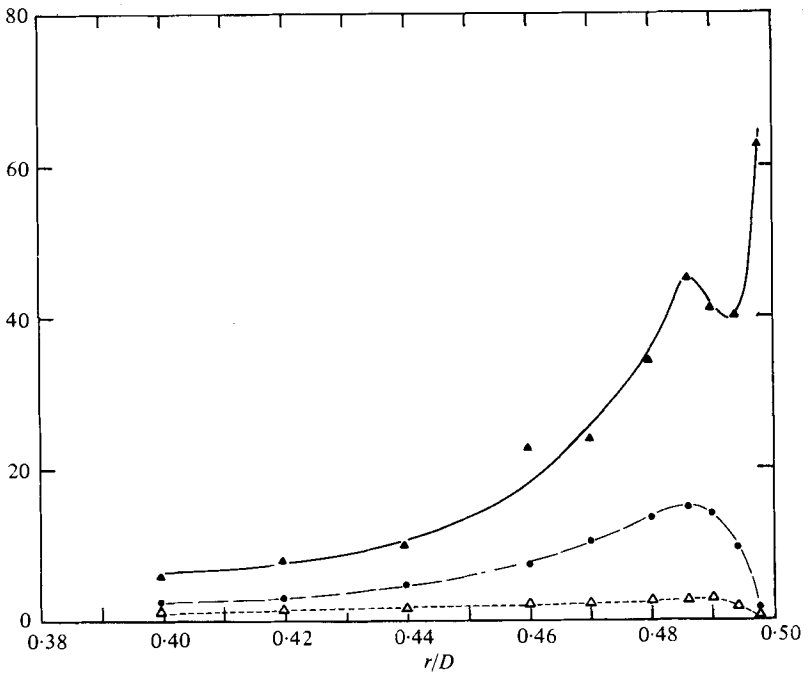

FIGURE 31. The principal components of the dissipation of turbulent energy. $x/D = 0$.

—▲—, $\frac{\nu D}{U_\tau^3}\overline{\left(\frac{\partial u}{\partial r}\right)^2}$; – –●– –, $\frac{\nu D}{U_\tau^3 r^2}\overline{\left(\frac{\partial u}{\partial \phi}\right)^2}$; · · · △ · · ·, $\frac{\nu D}{U_\tau^3}\overline{\left(\frac{\partial u}{\partial x}\right)^2}$.

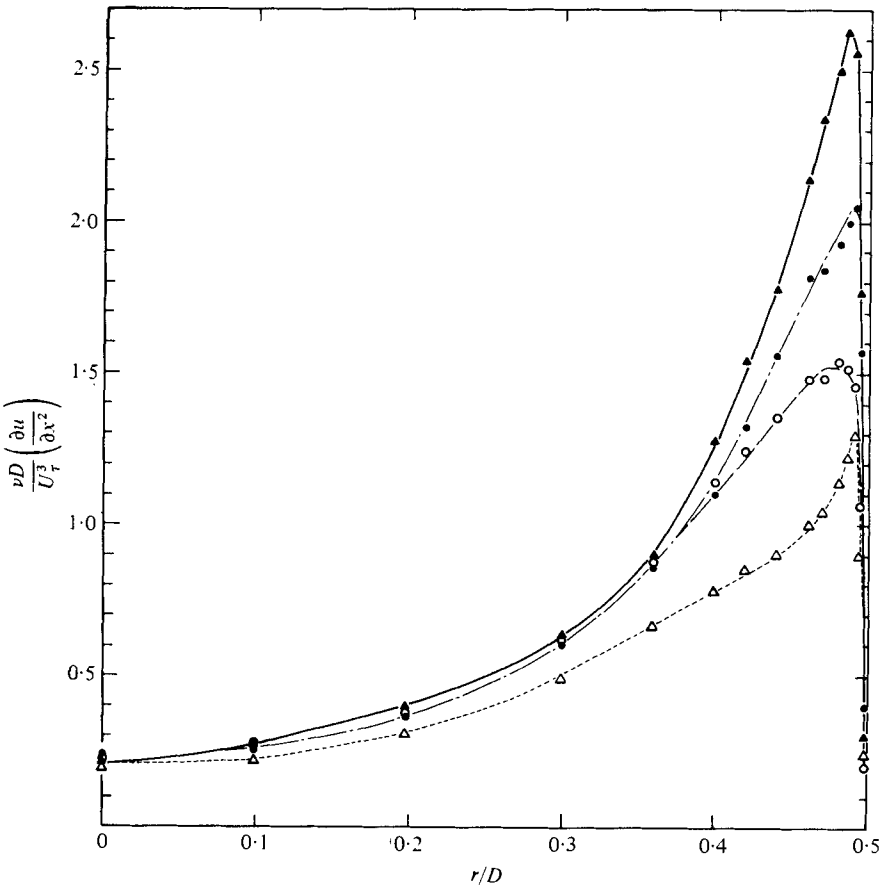

FIGURE 32. Distribution of the dissipative term $\overline{(\partial u/\partial x)^2}$. Symbols as in figure 8.

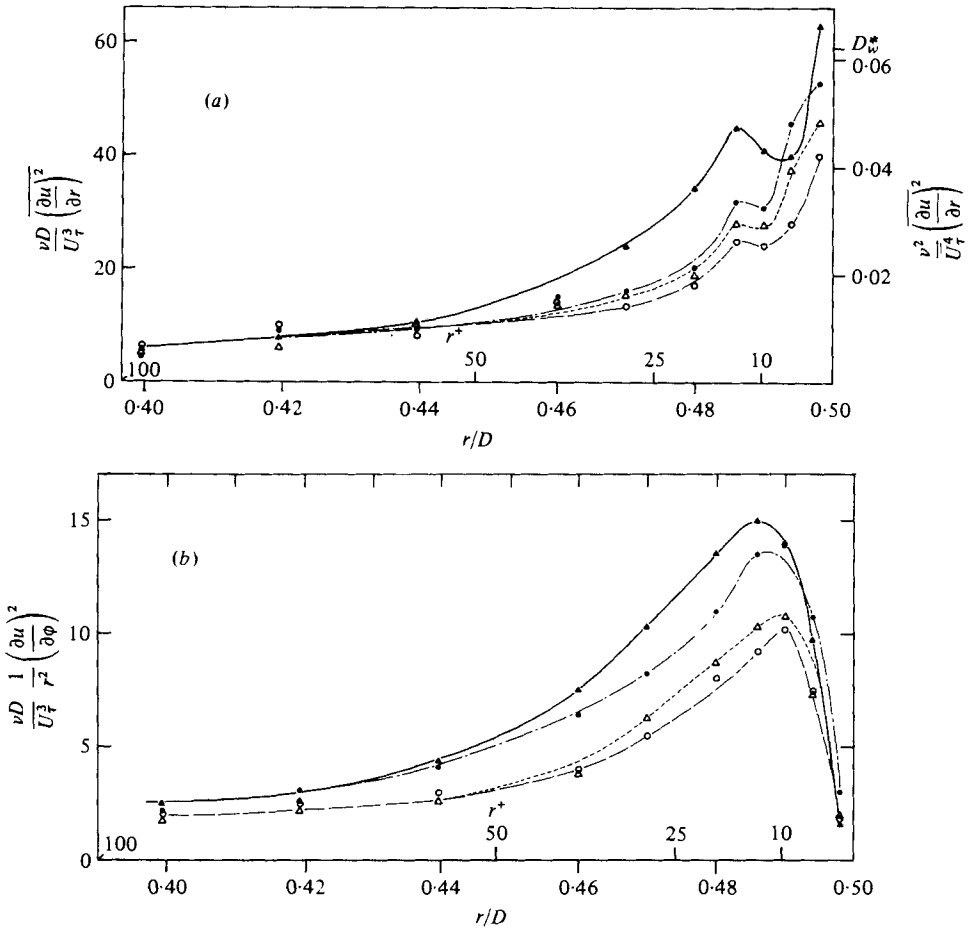

FIGURE 33. Distribution of (*a*) the dissipative term $\overline{(\partial u/\partial r)^2}$ and (*b*) the dissipative term $\overline{(\partial u/\partial \phi)^2}$. Symbols as in figure 8.

6. Conclusion and discussion

The radial distribution of each of the terms in the turbulent energy balance is reported for four axial locations in figures 34–37. Because the influence of suction does not penetrate the core of the flow, results are plotted only for the wall layers with the exception of those for the entrance plane, which corresponds to an undisturbed flow.

The results demonstrate that the turbulent energy balance is drastically altered by wall suction even though the Reynolds number is insignificantly reduced. The distribution of turbulent energy terms is similar for flows with and without suction; however the absolute magnitude of each of the terms in the critical wall layers is sharply reduced by the application of suction. Moreover the total turbulent energy production, integrated over the cross-section, is sharply reduced by the application of wall suction. This leads to the conclusion that the application of wall suction reduces the energy demanded from the mean flow. The attendant decrease in the measured values of the dissipation term confirm this.

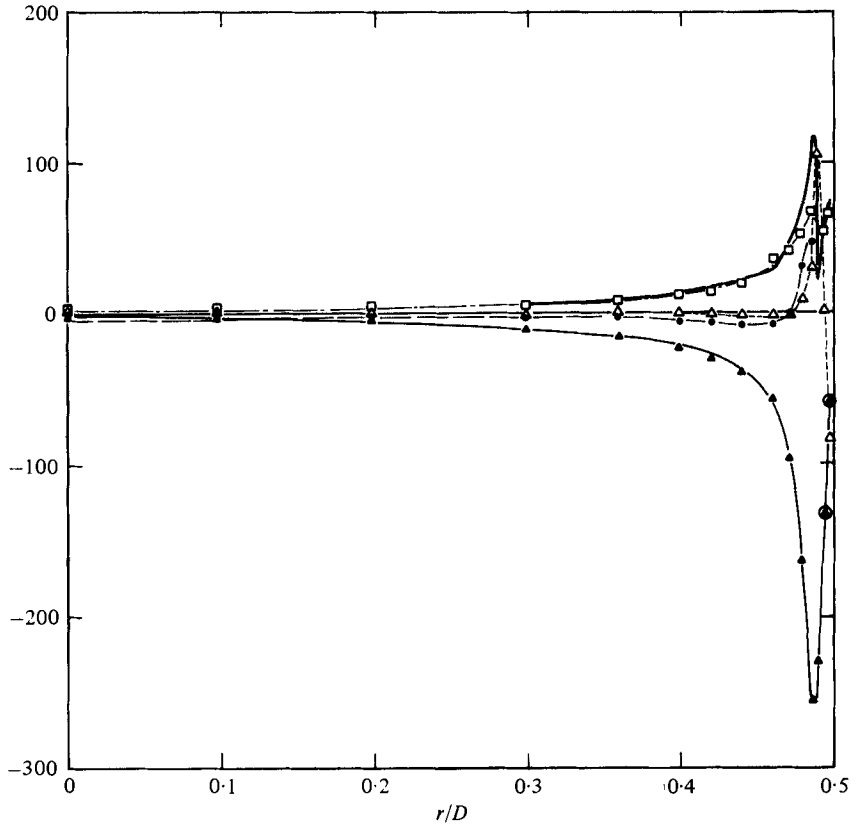

FIGURE 34(*a*). For legend see next page.

In examining the mechanisms within the suction section, it is convenient to recognize two regions in the flow field. In the first, extending from the entrance plane to about $x/D = 0{\cdot}5$, large radial mean velocities are produced and as a consequence large streamwise gradients in the mean flow produce significant additional terms in the energy equation and may not be neglected. Examination of the distribution of turbulent energy convection in the region $0{\cdot}1 \leqslant x/D < 0{\cdot}2$ shown in figure 28(*b*) reveals that an important mechanism in the reduction of turbulent kinetic energy is the transport of fluid containing this energy towards the wall. Since the boundary conditions do not permit this energy to pass through the wall it must be dissipated, probably in the neighbourhood of the maxima in the convective flow. Additional evidence supporting this conclusion is provided by the fact that the convection term has the same sign as the production term and hence the sum must be balanced by a term of opposite sign, the dissipation term.

In the second region in the flow, extending downstream from $x/D = 0{\cdot}5$, the radial and axial mean velocity components are small compared with the fully developed flow and may be neglected. Characteristic of the flow in this regime is a very small convective term, smaller even than that measured at the entrance plane, i.e. for a fully developed turbulent pipe flow without suction. Also characteristic of this region is a marked reduction in the maxima of the various energy terms in the wall layers.

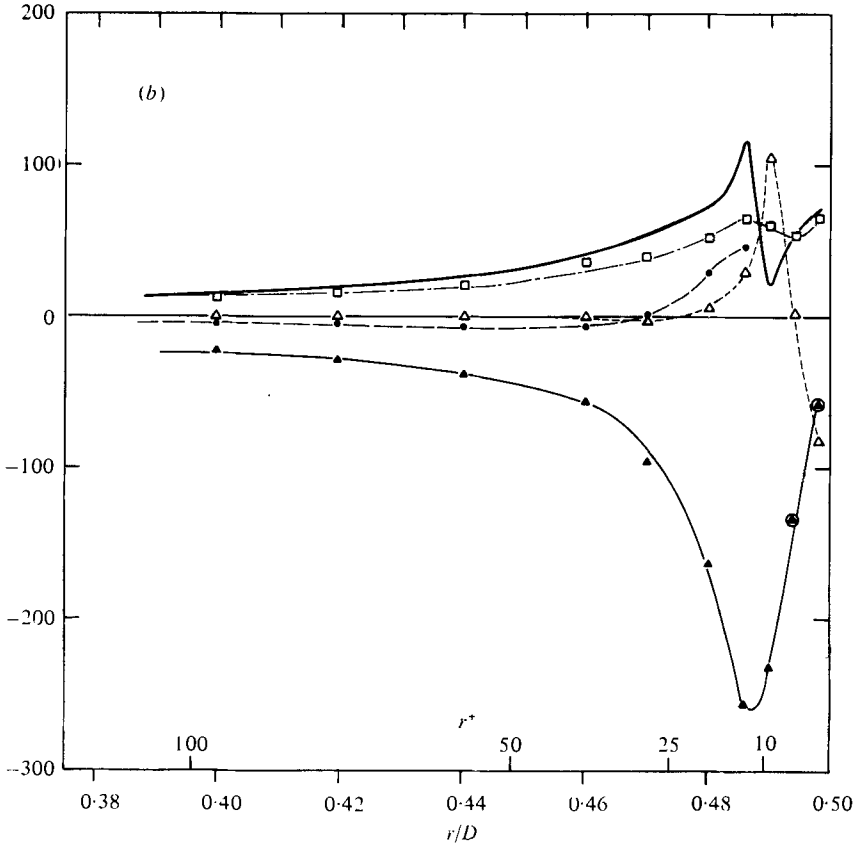

FIGURE 34. Turbulent energy balance at the entrance plane $x = 0$. (*b*) shows the wall layer on a larger scale. —▲—, PROD; —··■··—, CONV; – – ● – –, GDIF; · · · · △ · · · ·, DIF; —·□·—, DISM; ——, R.

The measured distribution of turbulent energy at the entrance plane, corresponding to a fully developed turbulent pipe flow, is compared with the results reported by Laufer (1953) in figure 38. Laufer's measurements were carried out at a Reynolds number of 5×10^4, about three times greater than that of the present work. The quantities compared in figure 38(*a*) were obtained from direct measurements without any interpretative assumptions. The results for the rate of turbulent energy production are in good agreement with minor differences in the neighbourhood of the maxima. The measurements of the distribution of the gradient diffusion term are also in good agreement. The turbulent kinetic energy diffusion rate is qualitatively similar but the absolute values reported here are somewhat smaller.

The dissipation and 'remainder', or unbalance, terms are shown in figure 38(*b*). Although Laufer measured the same quantities in the dissipation term as the present authors he estimated the unmeasured terms by assuming local isotropy, which is not appropriate in the wall layers. Thus in the present work the unmeasured portion of the dissipation has been lumped together with the pressure correlations and the dissipation and remainder terms are not directly comparable. Nevertheless the sum of these two terms may be compared directly and the results are in quite good agree-

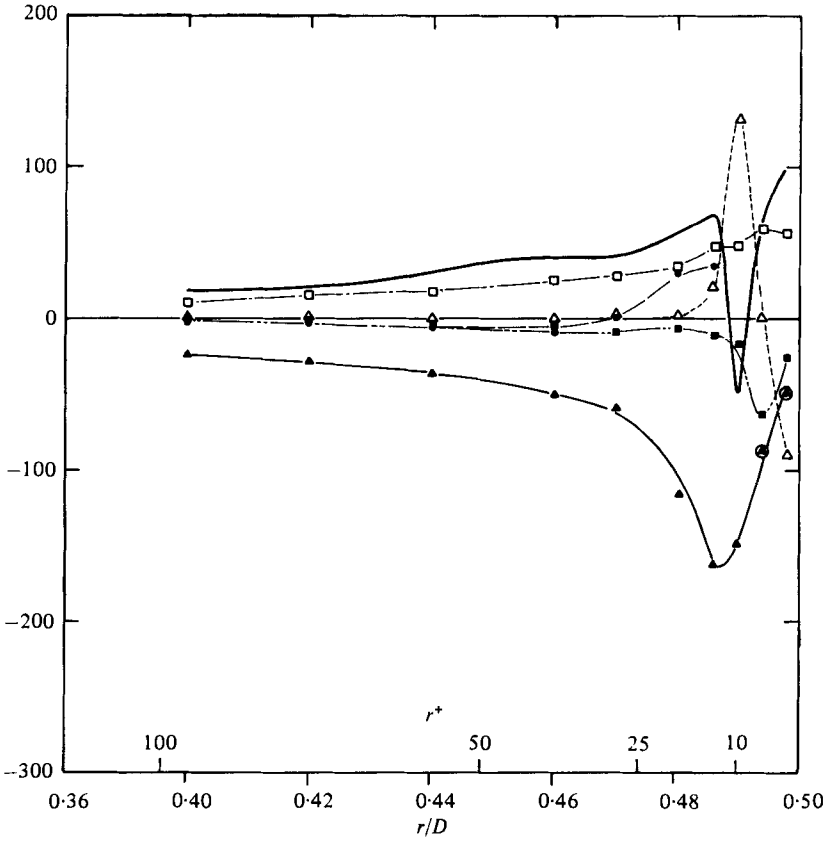

FIGURE 35. Turbulent energy balance at $x/D = 0{\cdot}503$. Symbols as in figure 34.

ment except in the neighbourhood of the maxima in Laufer's results. Note especially the very close agreement at the wall.

Differences in the neighbourhood of the wall between the present data and those of Laufer seem to be traceable to the fact that Laufer's data do not meet the wall boundary conditions. For example, the turbulent kinetic energy diffusion rate and turbulent pressure energy diffusion rate, which should vanish at the wall, retain finite values in Laufer's data while the dissipation term, which may have finite values at the wall, vanishes in Laufer's data.

The authors wish to express their sincere appreciation to Frl. G. Edel-Pils for helping to clarify a number of technical questions.

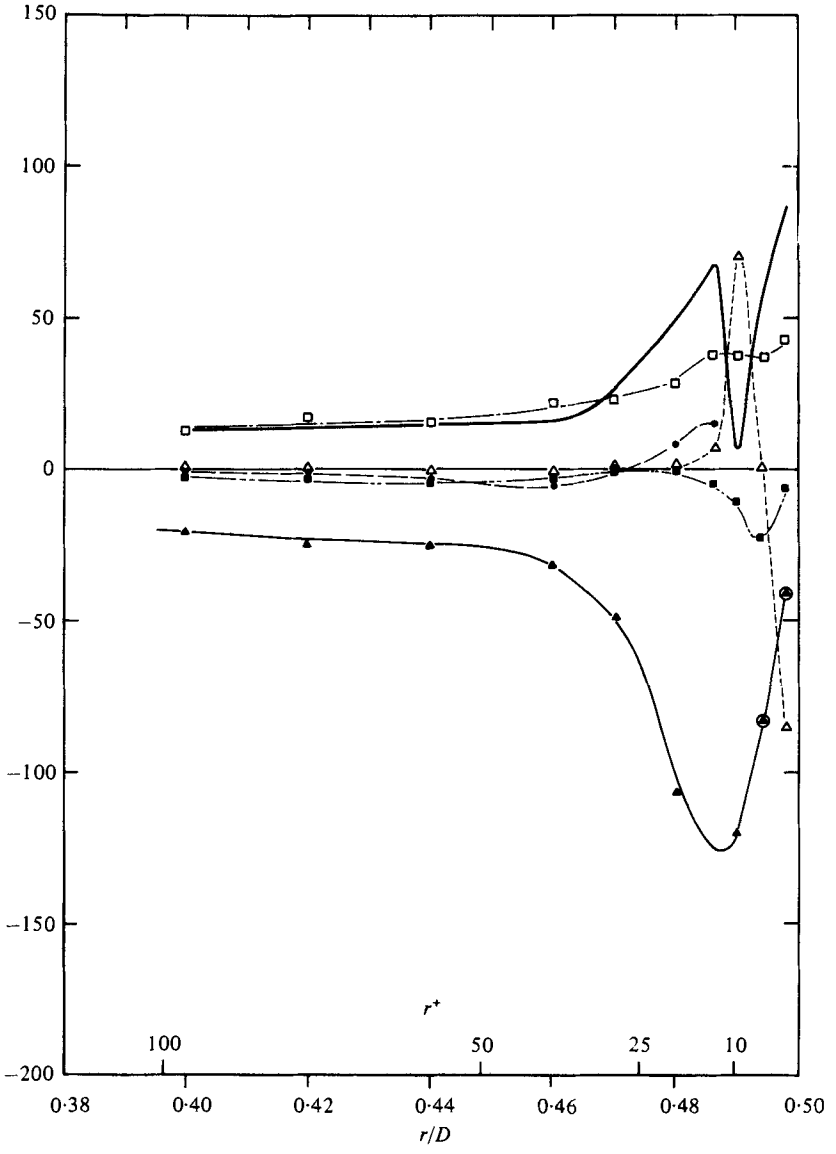

FIGURE 36. Turbulent energy balance at $x/D = 1{\cdot}358$. Symbols as in figure 34.

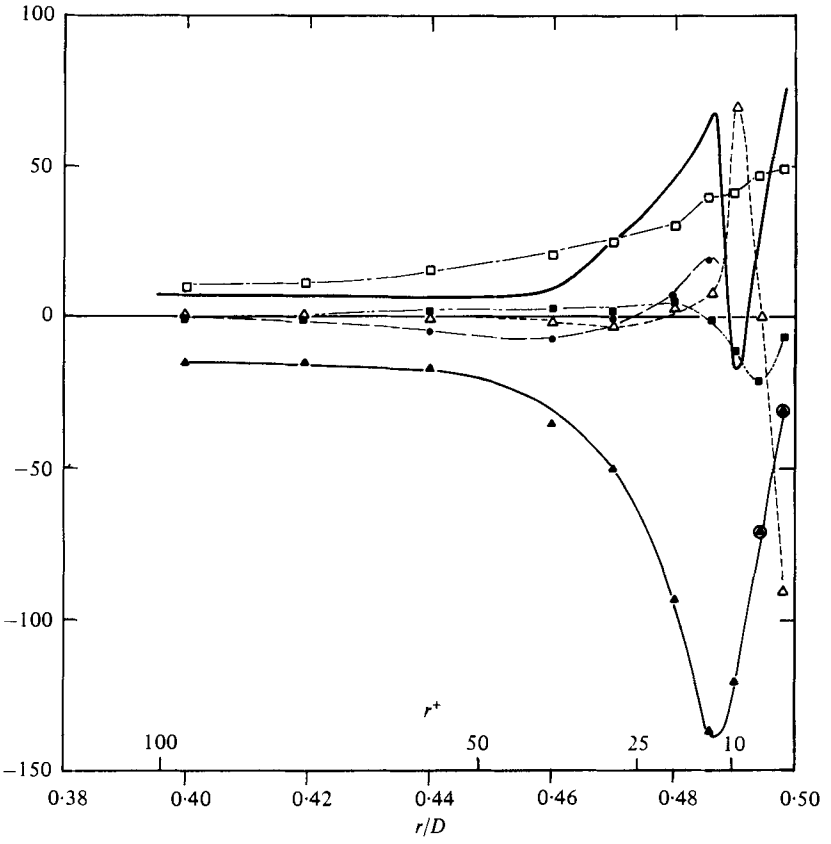

FIGURE 37. Turbulent energy balance at $x/D = 2{\cdot}213$. Symbols as in figure 34.

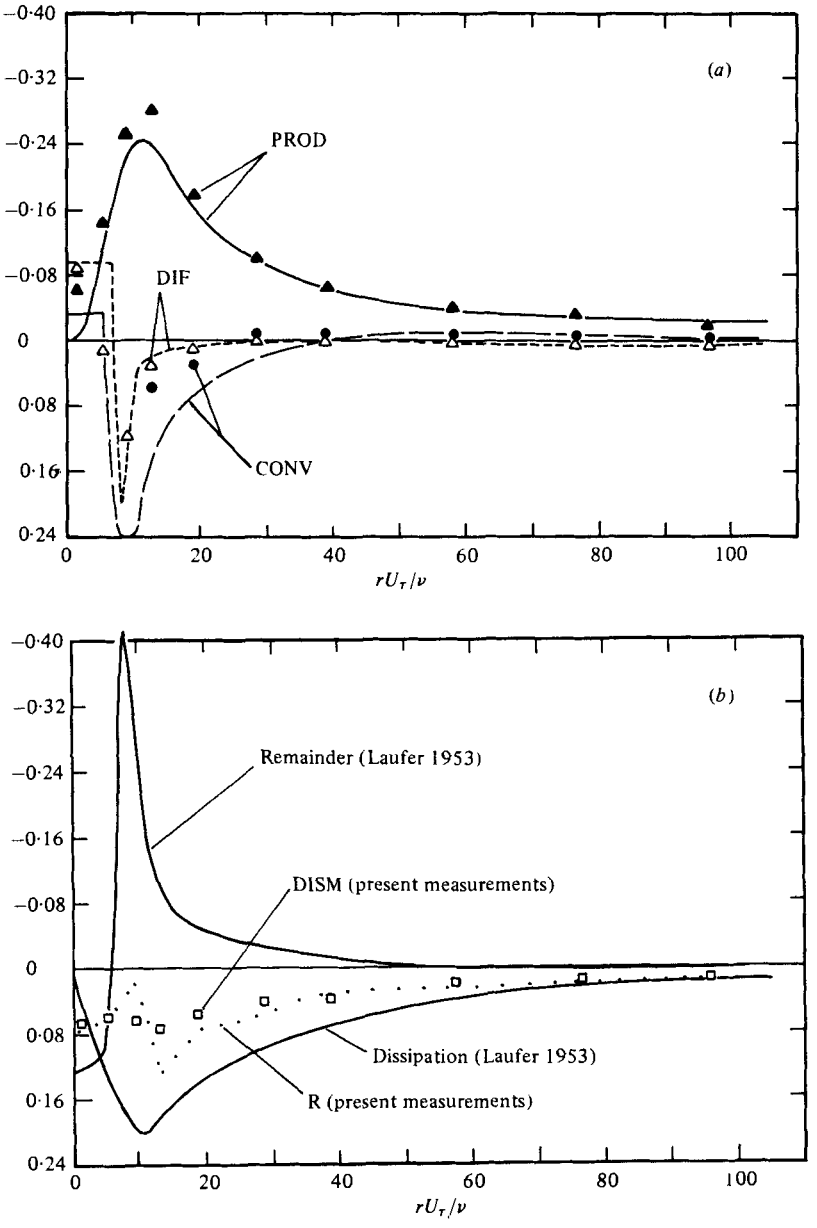

FIGURE 38. Comparison of measured (*a*) production and convection and (*b*) dissipation and remainder terms with those reported by Laufer (1953). In (*a*), the points represent the present measurements and the curves those of Laufer.

REFERENCES

AGGARWAL, J. K., HOLLINGSWORTH, M. A. & MAYHEW, J. R. 1972 Experimental friction factors for turbulent flow with suction in a porous tube. *Int. J. Heat Mass Transfer* **15**, 1585–1602.

AURELLI, A. 1967 Contribution à l'étude de l'écoulement turbulent dans une conduite cylindrique poreuse avec aspiration. *Publ. Sci. Tech. Minist. Air* no. 433.

BROSH, A. & WINOGRAD, J. 1974 Experimental study of turbulent flow in a tube with wall suction. *Trans. A.S.M.E., J. Heat Transfer* C **94**, 338–342.

COLEBROOK, C. F. & WHITE, C. M. 1937 Experiments with fluid friction in roughened pipes. *Proc. Roy. Soc.* A **161**, 367–381.

ECKELMANN, H. 1974 The structure of the viscous sublayer and the adjacent wall region in a turbulent channel flow. *J. Fluid Mech.* **65**, 439–459.

FAVRE, A. 1966 Couche limite turbulente sur paroi poreuse avec aspiration. *J. Méc.* **5**.

KINNEY, R. B. & SPARROW, E. M. 1970 Turbulent flow, heat transfer and mass transfer in a tube with surface suction. *Trans. A.S.M.E., J. Heat Transfer* C **92**, 117–125.

KREPLIN, H. P. 1976 Experimentelle Untersuchungen der Längsschwankungen und der wandparallelen Querschwankungen der Geschwindigkeit in einer turbulenten Rohrströmung. Ph.D. dissertation, Universität Göttingen.

LAUFER, J. 1953 The structure of turbulence in fully developed pipe flow. *N.A.C.A. Tech. Note* no. 2954.

MERKINE, L., SOLAN, A. & WINOGRAD, J. 1971 Turbulent flow in a tube with wall suction. *Trans. A.S.M.E., J. Heat Transfer* C **93**, 242–244.

ROTTA, J. C. 1966 Über die Geschwindigkeitsverteilung bei turbulenter Strömung in der Nähe poröser Wände. *Dtsche Luft- Raumfahrt Forschungsbericht* no. 66–45.

SCHILDKNECHT, M., MILLER, J. A. & MEIER, G. E. A. 1976 Energiegleichgewicht der turbulenten Nebenbewegungen in einer Rohrströmung mit Absaugung. *Mitt. Max-Planck-Inst. Strömungsforsch. Aerodyn. Versuchsanstalt.* (In press.)

TOWNSEND, A. A. 1947 Measurement of double and triple correlation derivatives in isotropic turbulence. *Proc. Camb. Phil. Soc.* **43**, 560–570.

WEISSBERG, H. L. & BERGMAN, A. S. 1955 Velocity and pressure distribution in turbulent pipe flow with uniform wall suction. *Heat Transfer Fluid Mech. Inst., Univ. Calif., Los Angeles* **14**, 1–30.